frontiers | Frontiers in Electronics

TYPE Review
PUBLISHED 01 September 2025
DOI 10.3389/felec.2025.1645594

OPEN ACCESS

EDITED BY
Zhenyi Zheng,
National University of Singapore, Singapore

REVIEWED BY
Yixin Shao,
Intel Corporation, United States
Youdi Gu,
Chinese Academy of Sciences (CAS), China

*CORRESPONDENCE
Zhiqiang Cao,
zhiqiangcao@buaa.edu.cn
Guodong Wei,
jellwei@buaa.edu.cn
Xueying Zhang,
xueying.zhang@buaa.edu.cn

†These authors have contributed equally to this work

RECEIVED 12 June 2025
ACCEPTED 31 July 2025
PUBLISHED 01 September 2025

CITATION
Zhao J, Bai L, Li S, Cao Z, Peng Y, Bai J, Cai X, Shi X, Lin X, Wei G and Zhang X (2025) An overview of advanced instruments for magnetic characterization and measurements.
Front. Electron. 6:1645594.
doi: 10.3389/felec.2025.1645594

An overview of advanced instruments for magnetic characterization and measurements

Junbiao Zhao[1†], Ligang Bai[1,2†], Shen Li[1†], Zhiqiang Cao[1,3*], Yi Peng[1,2], Jinrui Bai[2], Xudong Cai[1], Xinmin Shi[1], Xiaoyang Lin[1,2], Guodong Wei[1,2*] and Xueying Zhang[1,2,3*]

[1]State Key Laboratory of Spintronics, Hangzhou International Innovation Institute, Beihang University, Hangzhou, China, [2]Fert Beijing Institute, MIIT Key Laboratory of Spintronics, School of Integrated Circuit Science and Engineering, Beihang University, Beijing, China, [3]Truth Instruments Co. Ltd., Qingdao, China

Magnetic materials play a pivotal role in emerging fields such as new energy, information technology, and biomedicine, where accurate magnetic characterization is essential for material innovation and device engineering. Notably, with the burgeoning development of nanomaterials and spintronics, the importance of magnetic characterization has grown significantly, accompanied by increasingly higher requirements for precision and multi-dimensional analysis. This paper elaborates on the working principles and structural components of static magnetic measurement techniques—including Vibrating Sample Magnetometer (VSM), Alternating Gradient Magnetometer (AGM), Magneto-Optical Kerr Effect (MOKE) Microscope, Magnetic Force Microscope (MFM) and Superconducting Quantum Interference Device (SQUID) Magnetometer, as well as dynamic magnetic measurement techniques such as Alternating Current (AC) susceptometry and Ferromagnetic Resonance (FMR). In addition, this review also introduces emerging techniques relevant to spintronics, including Magnetometer based on negatively charged nitrogen-vacancy (NV^-) centers in diamond, Spin-polarized Scanning Tunneling Microscope (SP-STM), Lorentz Transmission Electron Microscope (LTEM), and Soft X-ray-based techniques, highlighting their principles and applications in quantum sensing, magnetic imaging, and element-specific spin analysis. This overview emphasizes the unique capabilities and measurement principles of each magnetic characterization instrument, providing users with practical guidance to identify the most appropriate tool based on specific research objectives, material properties, and experimental requirements, thereby improving characterization efficiency and accuracy.

KEYWORDS

magnetic characterization, spintronics, static magnetometry, dynamic magnetometry, macroscopic magnetic properties, magnetic domain imaging, frequency-dependent magnetometry

1 Introduction

Magnetic measurement, serving as a fundamental approach for investigating and characterizing the behavior of magnetic materials under external magnetic fields, plays an integral role in scientific research across numerous cutting-edge fields, including but not limited to biomedicine (Doaga et al., 2013; Nosrati et al., 2018; Kermanian et al., 2020), physics (Béa et al., 2008; Pan et al., 2008; Lavrijsen et al., 2013; Anbuselvan et al., 2021), and materials science (El-Bassuony and Abdelsalam, 2017; Ramakrishna et al., 2018; Jabbar et al., 2020). It enables the quantification of the magnetic parameters such as coercivity, remanent magnetization, and saturation magnetization (Cullity and Graham, 2011), as well as the evaluation of magnetic susceptibility and permeability, which reflect a material's responsiveness to magnetic fields. With continued research advancement, dynamic magnetic parameters—such as AC susceptibility, magnetic loss, magnetic relaxation (Topping and Blundell, 2018), and spin dynamic characteristics (Tang et al., 2023)—have become key indicators for understanding frequency-dependent behavior and microscopic magnetic processes. Moreover, the development of advanced characterization techniques, such as MFM, and NV center magnetometer, has enabled the exploration of nanoscale magnetic domain structures. In summary, magnetic measurements play an essential role not only in evaluating the performance of conventional ferromagnetic materials, but also in advancing research on novel magnetic materials, spintronic devices, and nanomagnetism.

Magnetic measurement instruments can be systematically classified into static magnetic measurement instruments and dynamic magnetic measurement instruments according to the state of the external magnetic field employed during measurement. Static measurement techniques operate under a constant or quasi-static magnetic field, and the representative instruments in this category include the VSM (Foner, 1959), AGM (Flanders, 1988), SQUID (Fagaly, 2006), MOKE-based magnetometer (Soldatov and Schäfer, 2017) and MFM (Krivcov et al., 2018), offering distinct advantages in sensitivity, spatial resolution, or suitability for specific sample forms and measurement conditions. In contrast, dynamic magnetic measurement techniques apply an AC magnetic field to probe frequency-dependent behaviors. Typical instruments include AC susceptometer (Topping and Blundell, 2018), which measure real and imaginary components of susceptibility over a range of frequencies, and FMR systems (Wang et al., 2018), which provide insights into damping mechanisms and spin dynamics at the microscopic level. In addition to conventional instruments, emerging techniques originally developed for spintronics—such as NV^- center magnetometer (Rondin et al., 2014), SP-STM (Bagchi et al., 2024), LTEM (Xue, 2025), and soft X-ray-based techniques (Van der Laan and Figueroa, 2014)—are increasingly used for high-resolution magnetic imaging and quantum sensing, offering access to spin structures at nanoscale levels. This classification reflects the progression of magnetic measurement from macroscopic, steady-state characterization toward microscopic, transient investigations, aligning with the evolving demands of modern magnetic materials research.

This review systematically introduces representative static and dynamic magnetic measurement techniques, while also covering spintronic-relevant emerging methods, aiming to serve as a practical reference for method selection and a source of inspiration for cutting-edge characterization development.

2 Static magnetic measurement techniques

Static magnetic measurement techniques serve as the cornerstone for elucidating the intrinsic magnetic behavior of materials, focusing on equilibrium magnetization responses under direct current (DC) or quasi-static magnetic fields. The magnetic hysteresis measurements (M-H curve) are conducted by sweeping an external magnetic field, enabling the characterization of key magnetic properties: M_s defines a material's maximum magnetization capacity, H_c quantifies its resistance to demagnetization, and M_r reflects retained magnetization. By measuring those key parameters, macroscopic magnetic characteristics—such as magnetization behavior and magnetism classification—can be effectively revealed and analyzed. Combined with temperature-dependent measurements, static techniques capture magnetic phase transitions, such as the Curie temperature (T_C) in ferromagnets or the Néel temperature (T_N) in antiferromagnets, revealing the onset of magnetic ordering. As a relatively fundamental yet powerful characterization approach, static magnetic measurement techniques play a vital role in both academic research and technological innovation. Their ability to reveal intrinsic magnetic parameters with high precision makes them indispensable for understanding material behavior and guiding the design of functional magnetic devices. In the following sections, we provide a detailed overview of several representative static magnetic characterization techniques, spanning from macroscale magnetization to nanoscale domain structures, with a focus on their principles, structures, and applications.

2.1 Vibrating sample magnetometer (VSM)

As one of the most widely utilized instruments for magnetic characterization, the VSM is renowned for its versatility, robustness, and adaptability to diverse sample forms, including bulk solids, powders (Frandsen et al., 2021), thin films (Ke et al., 2021), and liquids, whether in the form of single crystals, polycrystals, hard magnetic materials, or soft magnetic ones. This technique was first realized by Simon Foner in 1955 at the Massachusetts Institute of Technology (MIT) Lincoln Laboratory, where he constructed the first prototype using readily available materials, including a paper cup, paper straw, and a loudspeaker (Foner, 1996). The central idea was to mechanically vibrate a magnetized sample within a uniform magnetic field, thereby inducing an alternating magnetic flux through a set of stationary pickup coils. According to Faraday's law of electromagnetic induction, this time-varying magnetic flux generates an induced voltage (V_{emf}) in the coils that is directly proportional to the sample's magnetic moment. The corresponding experimental results were published in 1956 (Foner, 1956), and

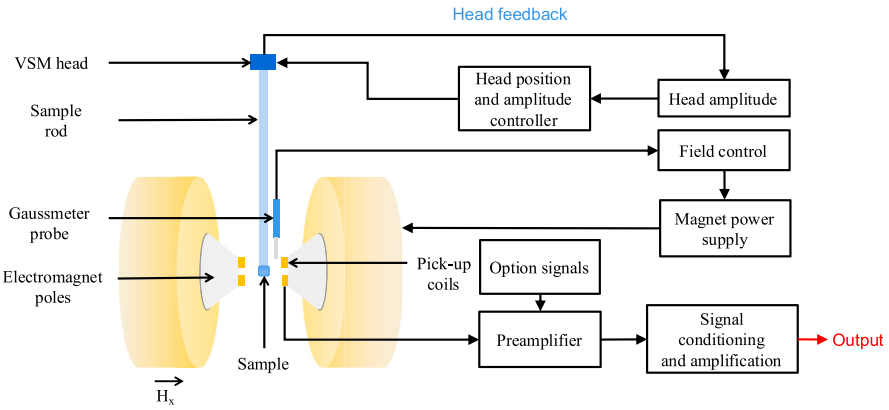

FIGURE 1
Induced voltage is produced when the sample mounted at the bottom of the rod vibrates perpendicular to the magnetic field, changing the magnetic flux in the pick-up coils fixed to the electromagnet poles. After being processed by the preamplifier, this voltage is output. The Gaussmeter probe is used to read and manipulate the magnetic field H_X, and the position-adjustable VSM head can be used to drive the rod and sample to vibrate.

further mechanical refinements followed in 1959. Subsequently, he granted the patent for the VSM design to Princeton Applied Research Corp (PARC), which marked the beginning of the commercial development of the VSM.

Over the decades, continued engineering and electronic advancements have significantly enhanced the sensitivity and stability of VSM systems. Modern commercial VSMs typically consist of three primary subsystems—the magnetic field generation and control unit, the vibration and sample mounting unit, and the signal detection and processing unit (as schematically illustrated in Figure 1)—and are capable of achieving sensitivities in the range of 10^{-7} to 10^{-8} emu with typical acquisition times of 10 s per measurement point. The magnetic field generation and control unit comprises an electromagnet and a gaussmeter. The electromagnet provides a uniform magnetic field to magnetize the sample, while the gaussmeter monitors the field intensity in real time. This feedback enables precise closed-loop control, ensuring the field remains stable and accurate throughout the measurement process. The vibration and sample mounting unit typically includes a vibration head, a sample rod, and the sample holder. The vibration head, driven by a mechanical oscillator, induces sinusoidal motion in the sample at a fixed frequency (commonly around tens of hertz). The sample, mounted at the lower end of the rod, is positioned within the uniform magnetic field. Vibration can occur either parallel or perpendicular to the field direction, depending on the system configuration (Mészáros, 2007). The signal detection and processing unit is mainly composed of a detection coil and a lock-in amplifier (LIA). The pickup coil system typically adopts a four-coil configuration arranged symmetrically along the vibration axis (Mallinson, 1966). This differential arrangement enhances the detection sensitivity and effectively cancels out background noise and environmental interference, thereby significantly improving the signal-to-noise ratio. As the magnetized sample oscillates within the magnetic field, it causes a time-varying magnetic flux through the pickup coils, thereby inducing a voltage via electromagnetic induction. The LIA, phase-locked to the vibration frequency, selectively amplifies and extracts the signal corresponding to the sample's magnetic response, effectively suppressing noise at other frequencies. By integrating these subsystems, the VSM enables accurate and efficient magnetic moment measurements across a broad range of material systems and sample geometries.

Further, digging into the working principle, the induced voltage V_{emf} obtained by the pick-up coils of the VSM can be given below (Dodrill and Lindemuth, 2021):

$$V_{emf} = mAfS$$

where, m denotes the magnetic moment of the sample, and A and f represent the amplitude and frequency of vibration, respectively, and S is the sensitivity function of the detection coils. It is clear from formula that increasing the amplitude A, the frequency f, or the sensitivity S will enhance measurement accuracy. However, in practical implementations, each of these parameters must be carefully optimized to avoid adverse effects. Excessive vibration frequency can induce substantial eddy currents in conductive samples, which in turn distort the magnetic response and generate undesirable heat. To mitigate these effects, the vibration frequency f is typically maintained below 100 Hertz (Hz). Similarly, to minimize geometric distortions and prevent signal loss due to non-uniform field coupling, the vibration amplitude A should be kept moderate, generally smaller than the diameter of the pickup coil. Furthermore, the sensitivity factor S can be enhanced through optimization of the pickup coil design, for example, by increasing the number of coil turns or modifying the coil geometry to better match the sample's magnetic field distribution. While increasing the number of turns improves inductive sensitivity, it also raises coil resistance, which elevates thermal noise and may reduce the effective signal-to-noise ratio. As an alternative, improving the magnetic coupling between the sample and the pickup coils, such as by reducing the coil-to-sample distance, offers a promising route to increasing S. It is important to note, though, that the spacing cannot be arbitrarily minimized, as sufficient room must be preserved for the sample to oscillate freely. Therefore, striking the perfect balance is crucial.

The distinctive advantage of the VSM over other magnetometers resides in its multifaceted applicability, enabling it to characterize samples across diverse morphological forms. For instance, VSM has been employed to characterize powder-form nanomaterials, such as $Ni_xCo_xMg_xCu_xZn_{1-4x}O$, where doping-dependent transitions from diamagnetic to mixed diamagnetic-ferromagnetic behavior were observed (Thien et al., 2024). It also enables the evaluation of perpendicular magnetic anisotropy (PMA) in thin film structures by analyzing their hysteresis loops (Smith et al., 2023). Furthermore, through modular integration of cryogenic and high-temperature accessories, the VSM facilitates magnetic measurements under controlled thermal environments, a capability particularly critical for studying temperature-dependent magnetic transitions. For example, Feng et al. (2023) employed a VSM to measure the temperature-dependent magnetization and hysteresis loops of tetragonal and hexagonal Mn_3O_4 nanosheets. These measurement results were used to determine the magnetic phase transition, Curie temperature, and identify the ferromagnetic ordering and the origin of magnetism. These applications collectively highlight VSM's versatility in probing static magnetic properties across a broad range of sample types and environmental conditions.

Despite its widespread use, the measurement precision of conventional VSM systems presents limitations when characterizing ultra-weak magnetic signals, particularly in the context of micro- and nano-electronic materials. In response, recent efforts have been devoted to improving system performance through the development of enhanced vibration drivers and more sensitive detection coil designs (Niazi et al., 2000; Nizhankovskii and Lugansky, 2007; El-Alaily et al., 2015; Jordán et al., 2018; Lopez-Dominguez et al., 2018; Dodrill and Lindemuth, 2021). While these customized, home-built VSM systems offer advantages in cost and user flexibility, they often fall short in achieving the high precision required for advanced magnetic analysis. Therefore, improving measurement precision and enabling versatile testing functions has emerged as a central challenge for the advancement of VSM technology.

2.2 Alternating gradient magnetometer (AGM)

As another key technique for magnetic moment measurement, the AGM offers significantly higher precision and sensitivity compared to the VSM, making it especially well-suited for characterizing materials with ultra-weak magnetic signals. Unlike VSM, which relies on detecting induced voltages via sample vibration, the AGM functions as a magnetic force balance, detecting vibration amplitude of a sample subjected to an alternating magnetic field gradient. The original concept of AGM emerged in the 1970s, where the sample was mounted on an elastic rod and subjected to an alternating magnetic field gradient. At resonance, the magnetic force induced a measurable deflection of the rod, visible under a microscope. The deflection amplitude was found to be proportional to the magnetic moment of the sample, establishing the foundation of the AGM technique (Zijlstra, 1970). Subsequent developments in AGM technology primarily focused on enhancing the vibration detection methods and refining the sample holder design. In 1980, the integration of piezoelectric bimorphs and lock-in amplifiers markedly improved detection precision, reaching a sensitivity of 10^{-10} emu (Roos et al., 1980). Building upon these advancements, Richter et al. (1988) refined the system through optimizing signal acquisition, introducing background noise compensation, and implementing strategies to suppress external interference, thereby achieving a remarkable sensitivity of 10^{-11} emu. Most notably, Todorovic and Schultz (1998) employed a quartz tuning fork as the piezoelectric sensor in combination with a magnetic field gradient of 5 kOe/cm (50 T/m), attaining a noise floor as low as 10^{-12} emu, one of the most sensitive performances reported to date in quantitative magnetic characterization.

Currently, commercial AGMs, based on Flanders' research (Flanders, 1988; 1990), utilize piezoelectric bimorphs as sensors, offering advantages such as high sensitivity, improved signal stability, and reduced noise interference, with a typical sensitivity of 10^{-8} emu at a sampling rate of one point per second. The Composition is schematically depicted in Figure 2A, and additional detail of probe is shown in Figure 2B. The core

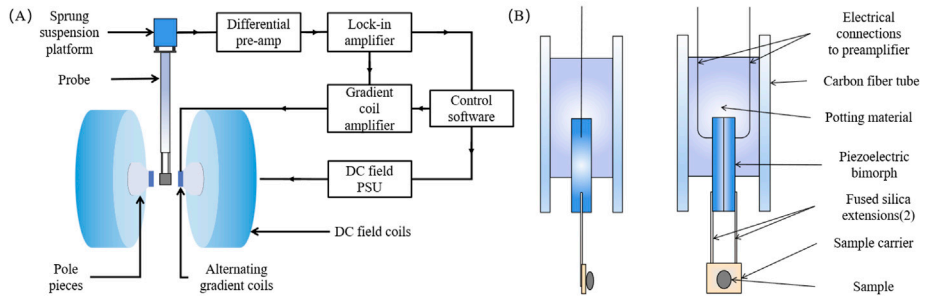

FIGURE 2
Schematic representation of an AGM. **(A)** The Basic structure and electronics. The magnetic sample, fixed at the bottom of probe and magnetized by the DC field, would vibrate along the direction of the gradient field which is caused by the alternating gradient coils. The probe converts the sample-induced vibration into an electrical signal, which is subsequently processed by the preamplifier and lock-in amplifier before being sent to the control software. **(B)** The detail of the probe and force sensor. The sample is mounted on a glass carrier connected to the piezoelectric bimorph through two fused silica extensions. The piezoelectric bimorph detects the vibration of the sample, generating the electrical signal which is proportional to the force on the sample.

sensing element of a typical AGM probe is a piezoelectric bimorph, which serves as a high-sensitivity vibration detector. The bimorph is mechanically coupled to the sample via two fused silica extensions, and the sample itself is mounted on a glass sample holder. The magnetic field system comprises a field-controlled electromagnet that provides a constant direct current (DC) magnetic field, along with gradient coils that generate an AC magnetic field. Under the excitation of the AC gradient field, the sample experiences a force at the same frequency as the alternating field, which causes the bimorph to generate a voltage signal proportional to the applied force. This signal is detected and extracted by a LIA. When a DC magnetic field is applied, the vibration amplitude of the sample is proportional to its magnetic moment. By measuring the vibration amplitude as a function of the applied DC field, a hysteresis loop can be obtained. For an AGM, the force on the sample in the non-uniform magnetic field is given by the following formula (Dodrill and Reichard, 2021):

$$F_x = m_x\left(\frac{\partial H_x}{\partial x}\right) + m_y\left(\frac{\partial H_y}{\partial x}\right) + m_z\left(\frac{\partial H_z}{\partial x}\right)$$

In general, a force in the X direction results from the gradient of the X component of the gradient field H_X interacting with the X component of the magnetic moment in the sample. The first term in equation is this force. The magnetic moment m_X can be estimated by measuring the magnitude of the field gradient and the alternating force. The second and third terms in equation should be decreased because they are undesirable. In normal situations, this is accomplished by lowering the field gradient.

The AGM has gained widespread recognition for its high sensitivity and precision in characterizing weak magnetic materials, making it a reliable tool for detecting subtle magnetic responses. For example, Şuan et al. (2020) utilized AGM to examine the impact of Al_2O_3 addition on Fe_3O_4 nanoparticles, demonstrating its capability to sensitively detect variations in saturation magnetization despite compositional changes. Similarly, Amir et al. (2023) used AGM to characterize superparamagnetic iron oxide nanoparticles (SPIONs) used in magnetic abrasives, extracting key parameters such as coercivity and saturation magnetization, and confirming their superparamagnetic behavior, which is critical for magnetically assisted polishing applications.

Through continuous optimization of mechanical sensing mechanisms, structural design, and gradient coil configurations, researchers have developed various AGM system variants tailored to different measurement demands. These advancements include integration with the MOKE (Hill et al., 1996), the development of vector magnetometers (Thomas et al., 2003), and specialized implementations for measuring reversible parallel and transverse susceptibilities (Barbic, 2004). Additional adaptations have enabled operation under cryogenic conditions (O'Grady et al., 1993) and the development of reed-type AGM systems for compact, high-sensitivity applications (Frey et al., 1988). Despite its high measurement precision and wide adaptability, AGM still faces several technical limitations in practice. Its sensitivity is highly susceptible to environmental disturbances, which may degrade performance by an order of magnitude or more. Common external interferences include acoustic noise, air flow fluctuations, ambient temperature variation, electronic noise, and mechanical vibrations from nearby equipment or human activity. In addition, the mechanical fragility of AGM probes, particularly the fused silica extensions, necessitates careful sample mounting to avoid damage. To address these challenges and enhance detection accuracy, Truth Instruments Co., Ltd., has recently introduced a novel variant known as the Laser Alternating Gradient Magnetometer (LAGM). This system employs laser Doppler vibrometry to capture the oscillatory motion of the sample induced by the alternating magnetic gradient. Leveraging the ultra-high displacement resolution of laser interferometric sensing, on the order of picometer, the LAGM achieves higher measurement precision than traditional AGMs, with magnetic moment noise levels as low as 10^{-9} emu. In addition, the LAGM features a decoupled design in which the vibration generation and detection subsystems are physically separated. This modularity facilitates integration with external systems, such as low-temperature cryostats or electrical transport measurement platforms, enabling the construction of a multifunctional physical field characterization system. Such versatility positions the LAGM as a promising tool for future high-precision magnetometer applications.

2.3 Magneto-optical Kerr microscope

The Magneto-Optical Kerr Microscope is a specialized instrument renowned for its ability to provide real-time, high-resolution imaging of magnetic domain structures in a non-invasive and surface-sensitive manner. Its working principle is based on the magneto-optical Kerr effect, wherein the polarization state of reflected light is modulated by the magnetization of the sample. This effect was first observed by John Kerr in the 1870s (Kerr et al., 1877), and has since laid the foundation for a range of magneto-optical measurement techniques. Based on the magneto-optical Kerr effect, two main types of instruments have been developed: Kerr magnetometers for hysteresis loops measuring, and Kerr microscopes for magnetic domain structures imaging. Especially, the Kerr microscope stands out for its capability to visualize spatially resolved magnetic phenomena, making it particularly valuable in both fundamental magnetism studies and spintronic research.

The schematic sketch and the mechanism of the MOKE are shown in Figure 3A. By measuring slight changes in the polarization of a polarized laser beam upon reflection from the sample surface, the magnetic information of the sample can be obtained (McCord, 2015). We can use this phenomenological model to describe the detailed origin of this effect. First, the linearly polarized light can be seen as a superposition of left and right circularly polarized components. Upon interacting with a magnetized sample, two distinct effects occur: (i) the two polarized components will travel with different velocities and they emerge at the end of the media with different phase shifts, which will lead to the Kerr rotation θ_k; (ii) the absorption coefficients of the two components for the magnetic media is different and they emerge at the end of the media with different intensities, which will lead to the Kerr ellipticity ε_k of the outgoing light (Ciprian et al., 2018). A further underlying reason for this phenomenological model is the Zeeman exchange splitting together with spin-orbit interaction, which is explained in detail in papers (Argyres, 1955; Bruno et al., 1996). Depending on the

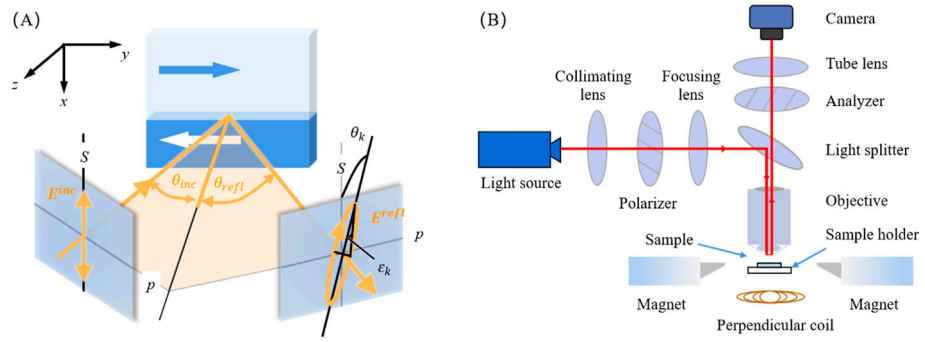

FIGURE 3
Illustration of the magneto-optical Kerr effect principle and a representative setup of Kerr microscope. **(A)** Magnetic measurement mechanism of MOKE. The linearly polarized light is incident on a magnetic material under an angle of θ_{inc} relative to the surface normal. As a result of the magneto-optical Kerr effect, the incident linearly polarized light E^{inc} undergoes a change in polarization state, and the reflected light E^{refl} becomes elliptically polarized. The resulting Kerr rotation θ_k and ellipticity ε_k are shown. θ_{refl} is the angle of reflection of light. **(A)** is adapted from McCord (2015). **(B)** Schematic diagram of a typical magneto-optical Kerr microscope setup. Linearly polarized light is focused onto the sample surface, and the reflected light undergoes a polarization change due to the magneto-optical Kerr effect. It is then analyzed by a beam splitter, compensator and analyzer before being captured by a camera. By varying the direction of the applied magnetic field relative to the plane of incidence and the sample surface, the system enables measurements of polar, longitudinal, and transverse Kerr effects. **(B)** is adapted from Cao et al. (2024).

relative directions of magnetization m and plane of incidence of the light, MOKE can be categorized into three geometries: polar MOKE, longitudinal MOKE, and transverse MOKE. Among them, polar and longitudinal MOKE are the most commonly used configurations. Polar MOKE is sensitive to the out-of-plane magnetization, where the magnetization vector is oriented normal to the sample surface. Longitudinal MOKE, on the other hand, detects the in-plane magnetization component that lies within the plane of incidence. In longitudinal MOKE measurements with oblique incidence, unwanted polar MOKE contributions may also arise, potentially affecting the accuracy of in-plane magnetization detection. To minimize the influence of the polar component and isolate the longitudinal response, several suppression strategies have been developed. These include a dual-configuration approach that swaps the laser source and detector to extract angular-dependent components via addition and subtraction (Ding et al., 2000), a quadrant-detector-based method that separates signals through spatially resolved analysis (Celik et al., 2019), and a recently developed mirror and quarter-wave plate configuration that leverages rotational symmetry to cancel the polar response (Greening et al., 2025). In addition, by combining any two or all of them and using some specified techniques (Vavassori, 2000; Ding et al., 2001), i.e., generalized magneto-optical ellipsometry, MOKE can provide the vectorial magnetic information of the sample. In summary, it should also be noted that, unlike techniques directly measuring magnetic flux or moment, MOKE signals depend also on the material-specific magneto-optical coupling strength.

The basic setup for detecting magnetism using MOKE typically consists of a light source, a polarizer, an analyzer, and a detector (Qiu and Bader, 2000). Linearly polarized light is incident on the surface of a magnetic sample; the reflected light is then collected by the detector after passing through the analyzer. To enable spatially resolved magnetic domain imaging, the Kerr microscope integrates a microscope objective and a camera into the optical path, as shown in Figure 3B. Additionally, to observe different types of MOKEs (e.g., longitudinal, transverse, or polar Kerr effects), aperture or fiber optic entry method can be used to adjust the incident light direction. While the use of a camera enables real-time visualization of magnetic domains, the quantitative accuracy of Kerr rotation angle measurements is generally lower than that of conventional point-detection MOKE magnetometers. This is primarily due to illumination instability, camera noise, and limited detector sensitivity, which reduce the precision of angle-resolved Kerr signal extraction.

Owing to its high spatial resolution, surface sensitivity, and non-destructive nature, magneto-optical Kerr microscope has become a powerful characterization platform for the investigation of magnetic domain structures and their evolution (Domenichini et al., 2019). One of its fundamental applications lies in defect detection and quality assessment of magnetic thin films, where high-resolution Kerr imaging enables precise magnetization mapping to identify local inhomogeneities and pinning sites (Adam et al., 2009; Adam et al., 2010). Similarly, MOKE has been widely employed to visualize magnetic skyrmions, nanoscale magnetic quasiparticles with topological protection, critical for next-generation low-power spintronic devices such as racetrack memories (Kato et al., 2023). Beyond static imaging, magneto-optical Kerr microscope plays a crucial role in the real-time study of magnetic domain wall dynamics, offering insights into the underlying mechanisms governing domain nucleation and propagation. In advanced configurations, MOKE systems can be integrated with electrical probe stations to facilitate the observation of domain wall motion driven by spin-transfer torque (STT) and spin-orbit torque (SOT) effects (Ryu et al., 2013).

To extend conventional MOKE techniques toward ultrafast magnetization dynamics, time-resolved magneto-optical Kerr effect (TR-MOKE) systems employ a pump-probe configuration to achieve picosecond and even femtosecond temporal resolution (Neudert et al., 2005; Mozooni et al., 2014). In this technique, two temporally separated laser pulses are used: a high-energy pump pulse excites the sample or initiates a specific magnetic event, while a delayed probe pulse monitors the resulting changes. By using a high-

precision displacement stage to systematically change the transmission distance of the probe pulse, the time delay between the pump and probe pulses can be gradually and precisely adjusted. This allows for the recording of time-resolved Kerr signals to reconstruct the dynamic evolution of the sample's magnetization (Schäfer and McCord, 2021). This enables the time resolution step of TR-MOKE to be as short as sub-picoseconds. Gradually, TR-MOKE microscope has become the main ultrafast magnetic dynamic measurement method in the field of spintronics, especially it plays an extremely important role in the field of optical-magnetic coupling such as all-optical switching (AOS) (Lalieu et al., 2019; Peng et al., 2024; Peng et al., 2023a; b; c). Researchers have employed TR-MOKE measurements to verify the ultrafast AOS dynamics in materials such as GdFeCo alloys (Kirilyuk et al., 2010), TbFe (Hassdenteufel et al., 2013), and Co/Gd multilayers (Lalieu et al., 2017), as well as the unique phenomena observed in antiferromagnetic materials like Mn_2Au (Bhattacharjee et al., 2018) and IrMn (Guo et al., 2024) under femtosecond laser excitation. Subsequently, TR-MOKE has also been utilized to explore the integration of AOS with magnetic tunnel junctions (MTJs) (Wang et al., 2022), as well as laser-induced magnetization switching in ferromagnetic spin valves (Igarashi et al., 2023; Igarashi et al., 2024). These studies offer novel approaches for the optical-electrical-magnetic integration and pave the way for future information writing and storage technologies. TR-MOKE is one of the most representative applications of ultrafast time-resolved pump-probe techniques. Beyond that, the advantages brought by pump-probe methods—such as ultrafast temporal resolution, multidimensional information, and non-contact measurement—have also been applied in various fields, including transient absorption, lattice and structural dynamics such as time-resolved X-ray diffraction (TR-XRD) and time-resolved Raman spectroscopy (TR-Raman), time-resolved ferromagnetic resonance (TR-FMR), and time-domain thermoreflectance for studying thermal properties.

MOKE technology has seen continuous advancements in recent years, driven by its exceptional sensitivity and scalability. Although quantitative characterization remains technically challenging, some researchers have proposed leveraging magnetic domain displacement as a potential solution (Hrabec et al., 2014; Magni et al., 2022). Moreover, in magnetic chip fabrication, wafer-level MOKE inspection has become the most prevalent method for quality control. Given these developments, MOKE-based techniques are expected to play an increasingly important role in both future research and industrial production.

2.4 Magnetic force microscope (MFM)

As another pivotal magnetic imaging technique, MFM has been widely adopted in both materials science research and industrial applications, owing to its ability to achieve nanoscale spatial resolution in the characterization of magnetic structures (Hartmann, 1999). It operates by detecting the magnetic force gradient between a magnetized probe tip and the sample surface, allowing for indirect imaging of magnetic field distributions with high spatial precision. Since its introduction, MFM has undergone continuous technological advancements and methodological refinements, establishing itself as a powerful tool for the high-resolution investigation of localized magnetic phenomena, including domain structures, magnetic coupling, and stray field distributions.

As illustrated in Figure 4A, MFM mainly consists of four key components: a cantilever, a ferromagnetic tip, a detection system, and a scanning control unit. The cantilever is usually made of silicon or silicon nitride, with a ferromagnetic tip attached to its end. The magnetic tips are typically fabricated from polycrystalline metal wires, such as nickel, iron, or cobalt. The detection system is responsible for measuring the subtle deflections of the cantilever induced by magnetic interactions between the tip and the sample.

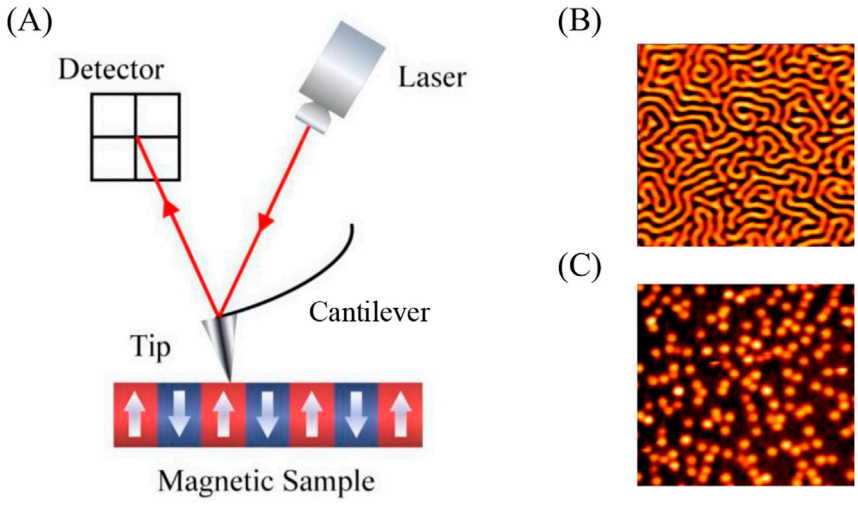

FIGURE 4
Principle and measurement images of MFM. **(A)** The measurement principle of MFM. **(B)** A typical MFM image of a labyrinth magnetic domain. **(C)** A typical MFM image of skyrmions.

Common detection approaches include optical beam deflection methods (Erlandsson et al., 1988; Rugar et al., 1988), capacitive sensors (Göddenhenrich et al., 1988), and in some high-sensitivity implementations, differential optical interferometry (Schönenberger and Alvarado, 1989). The scanning control unit precisely regulates the relative position between the sample and the tip, enabling high-resolution, point-by-point surface scanning and mapping of the magnetic force distribution at the nanoscale.

MFM operates based on the dipolar interaction between the ferromagnetic tip and the magnetic stray field of the sample surface. This interaction enables MFM to acquire both magnetic and topographical information of the sample simultaneously. As the ferromagnetic tip approaches the sample surface, the stray magnetic field of the sample exerts a localized force on the tip, leading to a measurable deflection of the cantilever. Highly sensitive detection systems are employed to accurately measure the slight displacements of the cantilever. These deflections provide quantitative information about the magnetic force distribution, thereby reflecting the underlying magnetization of the sample surface. The detected signal, typically proportional to the magnetic force or its spatial derivative, is integrated into a servo feedback loop that accurately regulates the tip-sample distance. During the scanning process, this distance is continuously monitored and recorded. As a result, an image representing contours of constant interaction force or force gradient is constructed, revealing critical magnetic features such as the size, shape, and orientation of magnetic domains. In addition to magnetic imaging, MFM can also operate in specific modes to acquire topographical information. For example, in the electrostatic control method, a controlled Coulomb force is applied between the tip and the sample in addition to the magnetic interaction force. By precisely adjusting the magnitude of this electrostatic force, the tip-sample distance is regulated. While keeping the total interaction force constant, the vertical displacement of the tip during scanning is recorded. This displacement data corresponds to the topographical variations of the sample surface, thus enabling topographical imaging. Figures 4B,C give typical domain images measured by MFM.

The diameter and geometry of the MFM probe tip have a critical impact on the instrument's spatial resolution. A larger tip radius increases the magnetic interaction volume, leading to signal averaging and a diminished ability to resolve fine-scale magnetic features. To address this limitation, several tip miniaturization techniques have been developed. Among them, electron beam deposition (EBD) (Jumpertz et al., 1997), focused ion beam (FIB) milling (Vasile et al., 1991), and the attachment of multi-walled carbon nanotubes (MWNTs) to microfabricated silicon cantilevers (Dai et al., 1996) have shown the most promising results. In addition, researchers have explored strategies to reduce magnetic coating coverage, such as selectively coating only the apex of the tip or thinning the magnetic layer, with the aim of enhancing magnetic sensitivity and spatial resolution. Beyond geometric and coating modifications, further advancements have led to the development of specialized probe types, including double-exchange tips (Han et al., 2007), antiferromagnetic tips (Liu et al., 2002), and synthetic antiferromagnetic tips (Wu et al., 2003). Measurement results indicate that these advanced probes can significantly improve the accuracy and fidelity of magnetic force measurements (Schwarz and Wiesendanger, 2008).

MFM leverages its sensitivity to local magnetic interactions to enable direct imaging of ferromagnetic domain structures, offering valuable insights into both hard and soft magnetic materials. It can resolve individual domain boundaries and reveal the fine internal features of magnetic domains, which are essential for understanding intrinsic magnetic properties (Göddenhenrich et al., 1988). In industrial applications, particularly within the magnetic recording industry, MFM serves as a key diagnostic tool (Martin et al., 1987). It is widely used to analyze the stray magnetic fields generated by recording heads, providing critical information for assessing their performance and structural integrity. Irregularities in stray-field distribution, for instance, may indicate mechanical defects or signal functional degradation (Van Schendel et al., 2001). Furthermore, MFM is applied to investigate written domains in both magneto-optical storage films and longitudinal magnetic recording media, thereby facilitating process optimization and contributing to higher data storage density and improved system reliability (Schoenenberger et al., 1991; Porthun et al., 1995). In recent years, MFM has served as a powerful tool for investigating a wide variety of magnetic structures. MFM has been widely applied to the study of patterned magnetic media (Rodríguez et al., 2016), artificial spin ice (Wang et al., 2016), domain walls (McCord, 2015), nanowires (Wohlhüter et al., 2015), multiferroic structures (Henrichs et al., 2016), and topological magnetic textures such as skyrmions (Pham et al., 2024). In particular, researchers have used MFM to demonstrate various spin current-driven operations (Pham et al., 2024; Mallick et al., 2024) of skyrmions, including their nucleation (Sun et al., 2023), motion (Pham et al., 2024), and annihilation (Mishra et al., 2025), which has significantly facilitated the development of skyrmion-based magnetic tunnel junctions (Chen et al., 2024) and racetrack memory devices (Wang et al., 2020). Meanwhile, quantitative MFM has also continuously evolved over the past 2 decades, employing a variety of approximation methods to quantitatively describe the two-dimensional stray field distribution of magnetic probes. These methods include parameter-free tip transfer function (TTF) approaches (Vock et al., 2011), the use of nitrogen-vacancy (NV) centers in diamond to measure the stray field and derive the cantilever calibration function (Sakar et al., 2021), and the approximation of the tip using a tip-equivalent magnetic charge model to decouple the stray fields of the sample and the probe (Feng et al., 2022a), among others. The two-dimensional stray field distribution of the sample obtained via quantitative MFM can reveal high-resolution, quantitative magnetic information such as the domain structure and the distribution of exchange bias fields (Zingsem et al., 2017). In addition, Monte Carlo (MC) methods have been introduced to analyze uncertainty propagation in quantitative MFM, providing a statistical framework for evaluating the reliability of measured magnetic parameters (Marschall et al., 2022). Moreover, an implementation that integrates specially engineered low-stiffness cantilevers, high-aspect-ratio magnetic nanowire tips, and multi-mode vibration excitation and control has demonstrated significant advantages in studying complex magnetic samples (Freitag et al., 2023). In the future, it is expected to become an important tool for high-resolution magnetic measurements.

MFM offers a series of significant advantages that make it a powerful tool in the study of magnetic materials. It exhibits high environmental adaptability, capable of operating under diverse

conditions with minimal sample-preparation needs, which simplifies experimental workflows across various fields. Moreover, its ability to concurrently acquire topographical and magnetic stray-field information provides a comprehensive view of the sample in a single scan, enhancing research efficiency. However, MFM also faces several drawbacks. Its resolution and performance are limited by the cantilever's sensitivity, which may be insufficient to detect subtle forces. In addition, environmental noise, such as temperature fluctuations and mechanical vibrations, and tip-induced stray fields can further interfere with measurements, especially for soft magnetic samples. These limitations collectively hinder the high-precision measurement capabilities of MFM and must be carefully addressed. With ongoing technological advancements, MFM continues to evolve toward higher precision and broader applicability, including capabilities such as quantitative magnetic moment analysis, image reconstruction and denoising, instrumental integration with complementary techniques, and exploration of emerging application fields (Kazakova et al., 2019; Feng et al., 2022b).

2.5 Superconducting quantum interference device-based magnetometer

Among various magnetic measurement techniques, SQUID magnetometer stands out as the most sensitive and precise instrument currently available. Utilizing the principles of superconductivity and the Josephson effect, SQUID can measure the magnetic moment with an accuracy of 10^{-8} emu in a strong magnetic field (7 T and above) and ultra-low temperature (1.8 K) environment (Schmelz et al., 2016). Due to its reliance on a superconducting state, SQUID magnetometer operation necessitates cryogenic environments, typically maintained by liquid helium or closed-cycle refrigeration systems, which leads to relatively high operational and maintenance costs. Nevertheless, SQUID remains unparalleled in its ability to perform ultra-high-precision magnetic moment measurements across a wide variety of materials and under complex experimental conditions (Weinstock, 2002), making it a critical tool in the study of low-dimensional quantum systems, superconductors, and spintronic materials.

The measurement structure and operating principle of the SQUID magnetometer are illustrated in Figure 5A. Each component in the system is carefully designed to serve the goal of ultra-high-precision magnetic moment detection. For example, the magnetic signal from the sample is first sensed by a pickup coil, designed according to Faraday's law of electromagnetic induction: as the sample moves relative to the coil, a time-varying magnetic flux induces a current that reflects the sample's magnetic moment. To further enhance sensitivity and suppress environmental noise, the system employs a balanced second-order gradiometer configuration in the coil design. In this design, both the upper and lower coils are wound clockwise, while the central coil is wound counterclockwise with twice the number of turns. This symmetric winding geometry effectively cancels out uniform magnetic field fluctuations and external magnetic interference, thereby significantly improving the signal-to-noise ratio of the system. Similar to the inductive coil design in VSM, the physical dimensions of the pickup coil in SQUID systems must also be optimized to balance sensitivity and geometric accuracy. On one hand, the gradiometer should ideally be small relative to the sample, so that magnetic flux lines do not return the pickup loop, maximizing magnetic coupling efficiency. On the other hand, to minimize artifacts caused by sample geometry and size variation, the detection coils are often made larger than the sample itself. This trade-off requires precise engineering, as improper coil-sample matching may introduce systematic errors in the measured moment, particularly if the sample deviates from the geometry used during system calibration (Kirtley et al., 1995; Stamenov and Coey, 2006).

In a closed superconducting circuit, the total magnetic flux enclosed by the circuit remains constant, a fundamental property governed by flux quantization. This means that any magnetic flux variation caused by the motion of a magnetic sample within the pickup coil must be compensated by an equivalent response elsewhere in the circuit. Through the design of a flux transformer, this flux variation can be coupled into the detection circuit, enabling indirect but highly precise measurement of the sample's magnetic moment. The SQUID is currently the most sensitive technology for magnetic flux detection. It can convert extremely small changes in magnetic flux into measurable voltage signals, and its core components are one or more Josephson junctions embedded in a superconducting loop. A Josephson junction is a classic "sandwich" structure consisting of two superconducting electrodes separated by an ultrathin insulating barrier, The behavior of the Josephson junction is governed by the Josephson effect, which manifests when the barrier thickness is less than the coherence length of the Cooper pairs in the superconductor. As illustrated in Figure 5B, when the current flowing through the junction is below the critical current I_C, the junction remains in the superconducting state, and no voltage drop is observed across it. Above the threshold current, the junction transitions into a resistive state and exhibits Ohmic behavior. The transition region near $I = I_C$ is particularly significant: small variations in current within this region result in large voltage responses. Based on the steepness of the slope in the transition region, the SQUID enables ultra-sensitive magnetic moment measurements (Fagaly, 2006).

Another key reason for the extremely high measurement accuracy of SQUID is the quantization characteristic when it measures magnetic flux. When the SQUID senses an external magnetic flux change Φ_a, it induces a compensating magnetic flux Φ_{ind} such that the total enclosed flux in the loop satisfies the condition $n\Phi_0 = \Phi_a + \Phi_{ind}$, where Φ_0 is the magnetic flux quantum and n is an integer. As shown in Figure 5C, the induced current changes as a periodic function with the external magnetic flux (Fagaly, 2006). To obtain an absolute and linear measurement of the flux value, an additional structure, known as a flux-locked loop (FLL), is introduced, as shown in Figure 5A. This configuration includes an external feedback voltage source that couples into the pickup coil and generates a compensating flux to actively cancel the flux change produced by the sample (Dumas and Hogan, 2021). The final output of the measurement is obtained by summing the feedback signal applied by the external voltage source and the residual high-precision signal extracted from the Josephson junction response, thus achieving both linearity and ultra-high sensitivity.

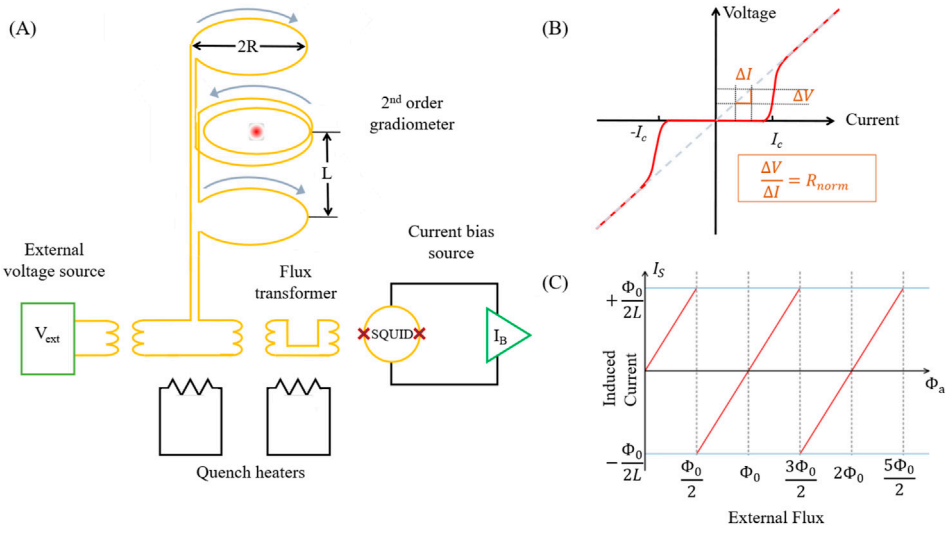

FIGURE 5
Schematic and characteristic response curves of a superconducting quantum interference device (SQUID) system. **(A)** Circuit diagram of the SQUID detection system. The sample passes or vibrates through the pickup coils on the left to produce a change in magnetic flux. The external feedback voltage source is used to counteract the absolute flux. The flux transformer couples the signal into the SQUID circuit, where the Josephson junctions (represented by crosses) respond sensitively to flux variations. The bias current $I_B = 2I_C$ ensures the junctions operate in the transition region for optimal sensitivity. **(B)** Generalized current-voltage (IV) response curve of a Josephson junction. The slope of the dotted line represents the resistance of the Josephson junction when it crosses the transition region. **(C)** The dependence of the current induced by DC SQUID with the external magnetic flux. The SQUID will generate the corresponding magnetic flux to make the total magnetic flux an integer multiple of the basic flux quantum Φ_0. Figure 5 is adapted from Franco and Dodrill (2021).

Depending on how the sample interacts with the pickup coil, SQUID magnetometers support two primary modes for magnetic moment measurement: the traditional DC scan and the SQUID-VSM mode. The key distinction between DC-SQUID and SQUID-VSM lies in their measurement modes: DC-SQUID operates in a static (DC) scanning mode, while SQUID-VSM employs a dynamic (AC) vibrating mode. This fundamental difference leads to diverging characteristics in terms of measurement targets, spatial resolution, sensitivity, and application focus. The traditional DC scan drives the sample completely through the second-order gradiometer. By fitting the recorded magnetic signal with position, the magnetic moment of the sample can be obtained. For example, Wu et al. (2021) utilized the DC measurement mode of SQUID to characterize the magnetic response of a superconducting sample, confirming its superconducting properties and magnetic shielding effect. In contrast, the SQUID-VSM mode keeps the sample oscillating sinusoidally at a fixed frequency near the center of the gradiometer, rather than translating it through the entire detection region. The time-varying magnetic response induces an AC voltage, which is measured using LIA, and the magnetic moment is extracted from the amplitude of the AC signal at the drive frequency (Hurt et al., 2013). For example, Adanlété Adjanoh et al. (2024) employed the SQUID-VSM mode to measure quasistatic magnetic parameters of Ta/Pt/Co/Pt ultrathin films, revealing that annealing significantly reduces coercivity and enhances magnetic domain structure. Due to the differences in underlying principles and measurement procedures, the two SQUID modes are suited to different types of samples and experimental needs. The DC scan mode determines the magnetic moment by fitting the spatial variation of the output voltage to a theoretical response function (Bouchiat, 2009), making it well suited for large or geometrically irregular samples, where positional correction through fitting improves accuracy. In contrast, the SQUID-VSM mode measures the amplitude of the induced AC voltage and is therefore more appropriate for high-precision measurements of small, geometrically well-defined samples, where stable harmonic motion ensures consistent signal generation.

Although SQUID magnetometer is renowned for its exceptional sensitivity and precision, it presents several practical challenges that must be carefully addressed during operation. The need for cryogenic temperatures increases both system complexity and operational costs, while also limiting measurement throughput and accessibility. Additionally, measurement accuracy can be compromised by flux creep, magnet hysteresis, and instrumental drift, necessitating systematic calibration and stabilization (Sawicki et al., 2011; Buchner et al., 2018). Furthermore, SQUID magnetometer is generally not suitable for large-volume or strongly magnetic samples, as these may exceed the dynamic range of the pickup coils or introduce nonlinearities and flux instabilities in the detection process. Nevertheless, due to its unparalleled capability for detecting ultra-weak magnetic signals and enabling absolute magnetic moment quantification, SQUID magnetometry remains one of the most widely adopted techniques in magnetic characterization. Ongoing advances such as cryogen-free cooling technologies, miniaturized SQUID-on-chip systems, and enhanced real-time feedback electronics continue to improve its usability and reliability, thereby expanding its applications in both fundamental studies and applied magnetism research.

3 Dynamic magnetic measurement techniques

Static magnetic characterization techniques reveal the equilibrium magnetic properties of materials under direct current fields, yet their quasi-static limit inherently fails to capture the dynamic behavior of magnetic moments in alternating electromagnetic fields. For investigations of high-frequency devices or spin dynamics, a transition to the dynamic measurement paradigm is necessitated, employing time-varying electromagnetic fields to excite forced magnetization oscillations or resonant spin precession, with theoretical interpretation based on the Landau-Lifshitz-Gilbert (LLG) equation to resolve frequency-dependent responses. This transition from equilibrium-state characterization to dynamic-state analysis not only addresses the limitations of static characterization but also establishes a spatiotemporal framework for material magnetism, providing critical insights for spintronics and high-frequency device applications.

3.1 Alternating current (AC) susceptometer

AC susceptometry is a fundamental technique in magnetism research and plays a central role in characterizing the dynamic magnetic responses of materials (Hartshorn, 1925). By quantifying the frequency-dependent magnetic susceptibility under alternating electromagnetic fields, this method provides crucial insights into phenomena such as superconducting phase transitions (Bałanda, 2013), magnetic relaxation processes (Mydosh, 1993), and energy dissipation mechanisms (Gatteschi et al., 2006). As a result, it offers a powerful tool for bridging the gap between a material's microscopic magnetic dynamics and its macroscopic functional properties.

The theoretical foundation of AC susceptometry lies in the response of materials to alternating fields, described by the complex magnetic susceptibility $\chi(\omega)$

$$\chi(\omega) = \chi'(\omega) + i\chi''(\omega)$$

Here, real part $\chi'(\omega)$ represents the in-phase magnetization component, while imaginary part $\chi''(\omega)$ quantifies out-of-phase energy dissipation arising from hysteresis, eddy currents, or spin-relaxation processes. This formulation assumes the weak-field approximation, under which the system exhibits harmonic responses confined to the fundamental frequency ω. A central framework for interpreting AC susceptibility is the Debye relaxation model (Topping and Blundell, 2018), which incorporates a damped dynamic equation to relate magnetization response to the characteristic relaxation time. This model reveals the frequency-dependent behavior of susceptibility (as shown in Figure 6A): at low frequencies, the magnetic response is fully developed; at high frequencies, the response is constrained by damping; and an energy dissipation peak emerges at intermediate frequencies, allowing precise interpretation of magnetic relaxation mechanisms in materials.

The mutual inductance method is a prevalent technique for AC susceptibility measurement, ideally suited for low-frequency regimes where magnetic relaxation and dynamic responses dominate, offering a simple yet robust solution for fundamental material characterization (as shown in Figure 6B). The system operates through a drive coil connected to an AC current source, generating a stable alternating magnetic field whose frequency and amplitude stability directly impact measurement precision. A sense coil array, typically configured with dual reverse-wound coils around the sample, detects magnetization-induced flux changes, converting magnetic responses into voltage signals and rejecting environmental noise. A lock-in amplifier then processes these signals using the drive coil current as a reference, applying phase-sensitive detection to extract in-phase and out-of-phase components from the fundamental frequency ω (Edgar and Quilty, 1993; Youssif et al., 2000). In practical measurements, the demagnetization effect must be considered. The internal magnetization of a material generates a demagnetizing field H_d opposing the external field H_{ex}, resulting in the internal field: $H = H_{ex} + H_d$. This leads to a discrepancy between the measured extrinsic susceptibility (χ_{ext}) and the intrinsic susceptibility (χ) of the material: $\chi_{ext} = \frac{\chi}{1+N\chi}$. Here, N denotes the demagnetization factor, determined by the sample geometry (Blundell, 2001).

AC susceptometry is widely employed to investigate the temperature- and field-dependent magnetic relaxation behavior of materials. In systems such as paramagnetic salts, it enables analysis of the spin relaxation process by applying the Debye relaxation model, which relates susceptibility responses to frequency under both isothermal and adiabatic conditions. By modifying this model to fit experimental data, researchers can elucidate the energy exchange mechanisms between spin systems and the lattice, thereby uncovering the underlying magnetic relaxation dynamics (Casimir and Du Pré, 1938). Furthermore, AC susceptibility has proven to be a powerful tool for probing superconducting phase transitions. For instance, by analyzing the temperature dependence of both complex and wide-band AC susceptibility under various flux pinning regimes, researchers have successfully extracted key physical parameters of high-T_C superconductors, including the critical temperature, magnetic penetration depth, and pinning potential, thereby providing deeper insights into the nature and dynamics of the superconducting transition (Gömöry, 1997). In recent years, AC susceptometry has been increasingly applied to study dynamic magnetic properties in advanced systems such as magnetic nanoparticles, molecular magnets, and low-dimensional heterostructures (Ghigo et al., 2022; Borgohain and Borah, 2021; Fernández-García et al., 2022). With sensitivity to both reversible and dissipative magnetic responses, it serves as a powerful tool for investigating spin dynamics and magnetic relaxation behavior. Notably, the development of high-frequency AC susceptometry has enabled time-resolved analysis of fast magnetic processes, including spin relaxation (Lah et al., 2020), quantum tunneling (Riordan et al., 2019), and high-speed switching relevant to spintronic devices (Cafolla-Ward, 2024). These advancements open new pathways for characterizing materials with short relaxation times and frequency-dependent losses.

However, this technology faces several challenges: during measurements, Joule heating and eddy current heating easily induce sample temperature drift, and existing temperature control measures show limited effectiveness under extreme conditions (e.g., high frequencies). Additionally, inductive and capacitive coupling noise in the environment interferes with detection signals, making interference suppression extremely difficult in complex electromagnetic environments. Moreover, the

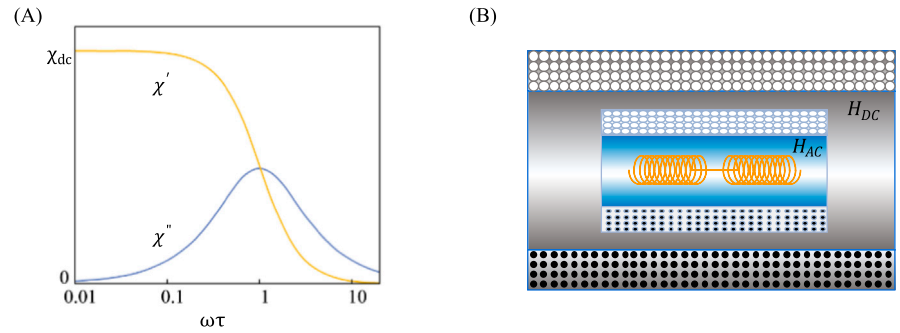

FIGURE 6
Principle and instrumentation of AC magnetic susceptibility measurement. **(A)** The Debye relaxation model describes the frequency dependence of the real (χ') and imaginary (χ'') components of AC susceptibility. **(B)** Schematic of a mutual inductance AC susceptometer. The system consists of two essential components: a drive coil (shown in blue) that generates an alternating magnetic field H_{AC}, and a detection coil (shown in yellow) wound around the sample to inductively measure the voltage response. A static bias field H_{DC} can also be applied externally. This configuration illustrates the spatial arrangement of excitation and detection coils, essential for understanding the AC susceptibility measurement principle.

absence of unified calibration standards reduces the comparability of results from different devices, while the diversity of standard samples also requires enhancement. In the future, AC susceptibility technology may further benefit from integration with multimodal magnetic characterization methods (e.g., Magneto-Optic Kerr Effect, X-ray Magnetic Circular Dichroism), enabling more comprehensive and element-specific analysis.

3.2 Ferromagnetic resonance (FMR)-based system

FMR is a widely used technique for probing the high-frequency magnetization dynamics of magnetic materials. In contrast to AC susceptometer, which characterizes low-frequency magnetic relaxation, FMR-based system investigates the resonant precession of magnetic moments induced by a combination of a static magnetic field and a microwave-frequency oscillating field. When the excitation frequency matches the natural precession frequency of the magnetization vector, resonance occurs, enabling quantitative investigation of properties such as magnetic anisotropy, damping constants, and gyromagnetic ratios. This makes FMR a vital tool in the study of spintronic materials, multilayer heterostructures, and magnetization relaxation phenomena under GHz-range excitations. The early exploration of FMR began in 1911, when V. K. Arkad'yev first observed microwave absorption phenomena in nickel and iron wires exposed to centimeter-wave radiation (Vonsovskii, 2013). In 1923, J. Dorfmann contributed to the theoretical interpretation of these observations and proposed experimental tests to investigate the influence of strong external magnetic fields on ferromagnetic resonance behavior (Dorfmann, 1923). The experimental realization of FMR advanced significantly in 1946, with pioneering work by James Griffiths (Griffiths, 1946), who is widely credited with its discovery. Soon after, Charles Kittel (Kittel, 1948) provided a theoretical explanation for Griffiths' results, laying the groundwork for the modern interpretation of FMR and its application across a wide range of magnetic systems.

To explain the fundamental principle of FMR, we need to start with a discussion on magnetic dynamics. Within the framework of the macrospin approximation, the time evolution of the magnetization vector ($\boldsymbol{m}$) of a ferromagnet in the presence of an effective magnetic field ($\boldsymbol{H_{eff}}$) can be effectively described by the Landau-Lifshitz-Gilbert (LLG) equation (Landau and Lifshitz, 1935),

$$\frac{\partial \boldsymbol{m}}{\partial t} = \left(-\gamma\mu_0 \boldsymbol{m} \times \boldsymbol{H_{eff}}\right) + \left(\alpha \boldsymbol{m} \times \frac{\partial \boldsymbol{m}}{\partial t}\right)$$

where γ, μ_0, and α are the gyromagnetic ration, vacuum permeability and the Gilbert damping parameterm respectively. The LLG equation includes two torque terms on the right-hand side. The first term, $-\gamma\mu_0 \boldsymbol{m} \times \boldsymbol{H_{eff}}$, describes precession and involves the rotation of both the magnetization vector ($\boldsymbol{m}$) and the effective magnetic field ($\boldsymbol{H_{eff}}$). The second term, $\alpha \boldsymbol{m} \times \frac{\partial \boldsymbol{m}}{\partial t}$, represents damping terms which aligns the magnetization along $\boldsymbol{H_{eff}}$. The value of α determines the damping rate, with larger values causing faster alignment and smaller values leading to slower alignment of m with $\boldsymbol{H_{eff}}$. The amplitude of the precessions gradually decreases due to damping in the ferromagnet. FMR occurs when an external alternating magnetic field (H_{RF}) is applied to the ferromagnet, compensating for the energy dissipation caused by damping. This results in a forced precession of $\boldsymbol{m}$. By tuning the frequency of H_{RF} to match the natural precession frequency of $\boldsymbol{m}$, the amplitude of the forced precession reaches its maximum due to resonance. This phenomenon is known as FMR, and the frequency of precession during resonance is referred to as the resonance frequency f ($f = \omega_{res}/2\pi$). Kittel's relation establishes a connection between the resonant field H_0 and the resonance frequency f,

$$f = \left(\frac{\gamma}{2\pi}\right)\sqrt{H_0\left(H_0 + 4\pi M_{eff}\right)}$$

where $4\pi M_{eff}$ is the effective demagnetization field of the ferromagnet. According to the equation, the resonance condition can be matched by fixing H_0 and tuning the frequency of H_{RF} or *vice versa*.

Early FMR measurements were primarily performed using resonant microwave cavities (Patton and Kohane, 1972), shown in Figure 7A, where the resonance condition was achieved by sweeping a static magnetic field while monitoring microwave absorption within a fixed-frequency cavity. These cavity-based

FMR setups offer high sensitivity due to their large quality factors, but their applicability is limited to discrete frequencies, requiring cavity replacement for frequency variation. To overcome this limitation, broadband FMR techniques were developed based on planar transmission lines (as shown in Figure 7B), such as coplanar waveguides (CPW) (Lee et al., 2009; Schäfer et al., 2012) and microstrip lines (Kalarickal et al., 2006; Kennewell et al., 2010), enabling continuous frequency coverage across a wide range (up to 65 GHz) (Wu et al., 2019; Khodadadi et al., 2020; Srivastava et al., 2020). These methods offer enhanced versatility, though they introduce challenges such as impedance matching, field nonuniformity, and increased microwave loss.

The Vector Network Analyzer (VNA)-FMR measurement is the most commonly used method for conducting broadband FMR experiments (Neudecker et al., 2006; Godsell et al., 2010). This method offers a simple experimental setup because the signal is generated and measured by the VNA in the same device. Figure 7C shows the configuration of the VNA-FMR experiment. The VNA typically operates in frequency-swept mode, while field-swept VNA-FMR measurements have also been reported in (Sharma and Kuanr et al., 2018; Tamaru et al., 2018). A key advantage of VNA-FMR lies in its ability to extract both the real and imaginary components of the complex susceptibility, enabling comprehensive magnetic characterization. However, careful full two-port calibration of the VNA system is essential to ensure measurement accuracy. As an alternative, broadband FMR can also be performed without a VNA using a modular scheme known as Phase-FMR (Montoya et al., 2014), illustrated in Figure 7D. This technique relies on direct power reflection measurements that are sensitive to frequency-dependent impedance changes. Therefore, these experiments typically require field sweeping at a fixed frequency to resolve resonance features accurately. Additionally, electrical detection of FMR has emerged as a sensitive method for probing resonance in magnetic structures (Tsoi et al., 2000; Kiselev et al., 2003). It relies on the generation of DC voltage at resonance, driven by effects such as spin-transfer torque and spin pumping (Sankey et al., 2006). Signals are acquired using voltmeters, with lock-in detection improving the signal-to-noise ratio. Owing to its high sensitivity, this method is well suited for studying nanoscale systems, including individual nanomagnets, and shows promise for integration into spintronic applications (Tulapurkar et al., 2005).

Ferromagnetic resonance (FMR) plays a central role in magnetic materials research by enabling the precise determination of key magnetic parameters. It allows accurate extraction of saturation magnetization via resonance conditions (Beik Mohammadi et al., 2019), and in-plane angular-dependent FMR measurements are widely used to analyze magnetic anisotropy, particularly in exchange-biased systems (Beik Mohammadi et al., 2017). In addition, broadband FMR techniques are essential for quantifying Gilbert damping constants, providing a powerful means to validate theoretical models such as Kambersky's torque correlation model, and to trace the microscopic origins of damping, including mechanisms governed by spin-orbit coupling. In recent years, FMR has also been extended to the *in situ* characterization of

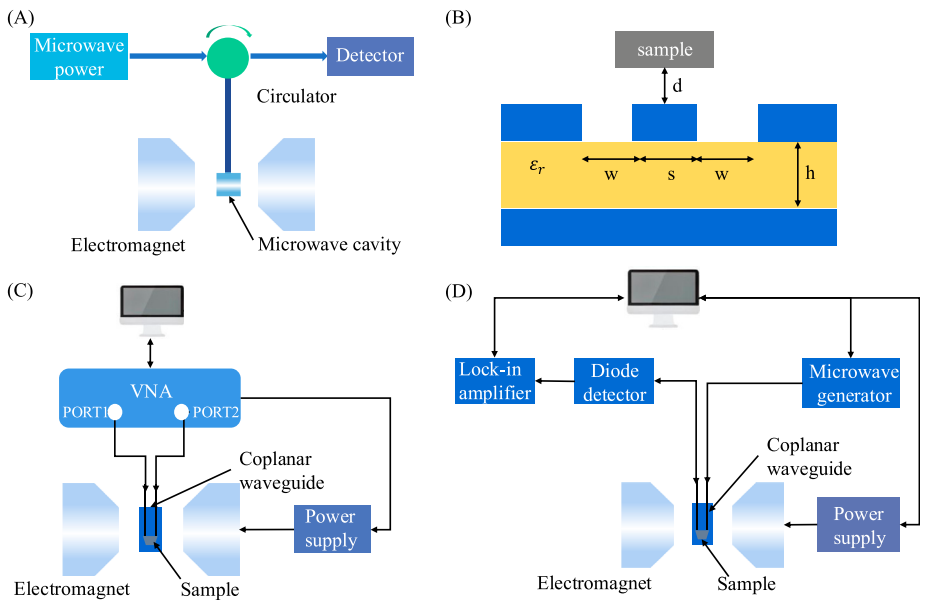

FIGURE 7
Schematics of different FMR. **(A)** Schematic of the cavity-FMR. The waveguide serves the purpose of supplying microwave power to the cavity where the sample is placed. It also functions as a path for the reflected signal from the cavity to reach the detector. To ensure proper signal flow, a circulator is employed. The circulator directs the reflected signal toward the diode while simultaneously safeguarding the generator from any reflected power. **(B)** Coplanar waveguide schematic with an additional ground plane on the substrate's back. The permittivity (ε_r) and thickness (h) of the substrate serve to characterize it. The signal trace is positioned parallel to the ground planes within the coplanar waveguide structure, has a particular width (s), and is spaced from them by a gap (w). A sample is positioned at a particular height (d) above the coplanar waveguide structure to measure or detect certain features. **(C)** Schematic of the VNA-FMR. In the VNA-FMR experiment, the coplanar waveguide is connected between the two ports of the VNA and placed within the electromagnet, which applies the static magnetic field. The magnitude of the applied field is controlled by a Power Supply. **(D)** Schematic of the Phase-FMR. The sample is excited by a microwave generator, and the power is detected using a diode detector and a LIA.

spin-orbit torque (SOT) devices, offering valuable insights into current-induced magnetization dynamics (Coester et al., 2023; Zhan et al., 2024). In such measurements, a radio-frequency current is applied to the device to excite magnetization precession via spin-orbit torques, and the resulting voltage signal—often referred to as the rectification voltage—is analyzed to extract key parameters (Kim et al., 2021; Chen et al., 2021). Specifically, by analyzing variations in resonance lineshape and linewidth induced by the applied current and magnetic field, researchers can determine the strength and angular dependence of spin-orbit torques, as well as quantify spin Hall efficiencies in multilayer structures (Hibino et al., 2024). This approach, known as spin-torque FMR (ST-FMR), has become a critical technique for optimizing spintronic device performance and for evaluating materials with strong spin–orbit interactions in magnetic random access memory (MRAM) and related applications (Chen et al., 2021). It has also been increasingly employed to investigate magnetization dynamics in two-dimensional magnetic materials, enabling the study of spin relaxation, damping, and anisotropy at the atomic thickness limit (Tang et al., 2023).

Furthermore, researchers have extended FMR by integrating it with complementary techniques to enhance spatial, spectral, and element-specific resolution. One such novel technique is X-ray detected FMR (XFMR) (Van der Laan and Hesjedal, 2023), which makes use of the XMCD effect to produce element-specific magnetic contrast in order to examine the dynamics of magnetization in individual layers. Variants such as diffraction-based FMR (DFMR) and reflectivity-based FMR (RFMR) extend XFMR by enabling the detection of magnetization dynamics through modulations in X-ray scattering and reflectivity signals, thereby enhancing structural and interfacial sensitivity (Burn et al., 2021). In addition, alternative non-microwave-based detection approaches have emerged, including the use of a MFM tip (Nazaretski et al., 2007a; Nazaretski et al., 2007b) and micro-focus Brillouin light scattering (BLS) techniques (Demidov et al., 2010; Demidov et al., 2011), both offering high spatial resolution and local FMR sensitivity. These hybrid and indirect detection methods broaden the experimental versatility of FMR, enabling investigation of complex magnetic phenomena in nanoscale systems.

4 Emerging spintronic characterization techniques

While static and dynamic magnetic characterization techniques remain foundational in understanding material magnetism, the rapid advancement of spintronic research has introduced new measurement demands. As spintronic systems often involve nanoscale spin textures, interfacial phenomena, ultrafast dynamics, and spin-polarized electronic states, traditional methods may face limitations in spatial resolution, temporal precision, or sensitivity to spin-specific quantities. To address these challenges, a range of emerging techniques has been developed—such as NV^- center magnetometry, Lorentz transmission electron microscopy (LTEM), Spin-polarized scanning tunneling microscope (SP-STM), and soft X-ray-based techniques. These tools provide localized, time-resolved, and often quantum-sensitive access to spin phenomena, and thus merit dedicated discussion distinct from conventional magnetic measurement systems.

Diamond-based magnetic sensing and measurement technologies are emerging quantum magnetometry techniques that have gained significant attention in recent years. These methods typically involve introducing various point defects into diamond crystals and utilizing the magnetic field sensitivity of their spin states for measurement. Diamond-based magnetometry includes techniques based on diamond color centers such as nitrogen-vacancy (NV), silicon-vacancy (SiV), and group-IV-related centers like GeV and SnV, among which the NV center technology is the most widely applied (Zhang et al., 2025; Guo, 2023; Hong et al., 2013). Magnetometer based on negatively charged nitrogen-vacancy (NV^-) centers in diamond has recently attracted significant attention as emerging quantum sensors in condensed matter physics (Rondin et al., 2014; Maze et al., 2008). This method relies on the Zeeman response of NV^- spin states to external magnetic fields (Barry et al., 2020). By applying green laser excitation and microwave pulses, the NV^- electronic spins can be initialized, manipulated, and optically read out. Specifically, when a local magnetic field is present, the spin levels split, resulting in changes in fluorescence intensity. The magnetic field strength and direction can then be precisely extracted via optically detected magnetic resonance (Rondin et al., 2014; Schirhagl et al., 2014). NV^- magnetometry offers nanoscale spatial resolution (Grinolds et al., 2014), exceptional field sensitivity (Grinolds et al., 2013; Sushkov et al., 2014) and compatibility with a wide range of environments—from room temperature to cryogenic conditions (Pelliccione et al., 2016; Liu et al., 2019) and from ambient to high pressure (Lesik et al., 2019). Benefiting from these capabilities, NV^- center magnetometry is widely used for nanoscale magnetic characterization, such as probing magnetic domains and spin textures (Dovzhenko et al., 2018). Beyond static structures, it has been employed to detect magnon excitations in antiferromagnetic materials, extending its application to systems without net magnetization (Heitzer et al., 2024). In addition, NV^- centers have been used to study dynamic processes such as the non-resonant detection of GHz-frequency domain wall oscillations using nanodiamonds positioned near magnetic structures (Xu et al., 2019).

Spin-polarized scanning tunneling microscopy (Bode, 2003), as a magnetic imaging technique with atomic spatial resolution, has been widely employed for investigating local spin structures in spintronic materials (Palotás et al., 2017). Its working principle relies on the spin dependence of the tunneling current, when both the STM tip and the sample surface are spin-polarized, the tunneling current is influenced not only by the local density of states but also by the relative orientation of their spin directions, thereby enabling the detection of local spin configurations. Benefiting from this mechanism, SP-STM retains the ultrahigh spatial resolution of conventional STM while providing additional sensitivity to spin states. Furthermore, by adjusting the magnetization direction of the tip, SP-STM allows for selective imaging of different spin components, enhancing its applicability to complex magnetic structures. At present, SP-STM is primarily employed for imaging spin textures and local magnetic structures (Bagchi et al., 2024; Corbett et al., 2022). It is particularly effective in investigating spin configurations and their control in

ferromagnetic and antiferromagnetic materials (Brüning et al., 2025; Spethmann et al., 2024), and has become a key technique for exploring the microscopic mechanisms of spintronic devices. Moreover, SP-STM has demonstrated unique capabilities in resolving chiral spin configurations, such as noncollinear spin spirals and skyrmion lattices, which are central to the study of Dzyaloshinskii-Moriya interaction-driven phenomena and topological spin textures (Brüning et al., 2025; Lee et al., 2022).

Lorentz Transmission Electron Microscopy (LTEM) is a powerful technique for high-resolution imaging of magnetic domain structures (Grundy and Tebble, 1968; Hale et al., 1959). It visualizes in-plane magnetization by detecting the deflection of electron beams caused by Lorentz forces as they pass through magnetic materials. LTEM typically operates in underfocused or overfocused imaging modes to enhance magnetic contrast and is particularly suitable for observing domain walls, magnetic vortices, and skyrmions (Xue, 2025; Chen et al., 2022). Compared with other magnetic imaging methods, LTEM offers real-space imaging with nanoscale spatial resolution and can be combined with *in situ* magnetic field and temperature control, enabling dynamic studies of magnetization processes and topological magnetic structures (Peng et al., 2018). For example, Matsumoto et al. employed LTEM to investigate the magnetic structure of a $Co_8Zn_8Mn_4$ alloy and identified a stable triple-q skyrmion phase, revealing the temperature- and field-dependent evolution of its topological magnetic textures (Kotani et al., 2016). However, LTEM also has certain limitations—it requires electron-transparent samples (typically thinner than 100 nm), is mainly sensitive to in-plane magnetization components, and must be conducted in high-vacuum TEM environments (Xue, 2025). These factors impose stringent demands on sample preparation and experimental setup.

With the development of X-ray magnetic circular dichroism (XMCD) and X-ray magnetic linear dichroism (XMLD), soft X-ray-based magnetic measurements using synchrotron radiation have become a key technique in magnetism research (Van der Laan and Thole, 1991; Schütz et al., 1987). These methods build on X-ray absorption spectroscopy (XAS), which provides element-specific and chemical-state-sensitive information by detecting the absorption of X-rays at specific energy edges (such as L_2 and L_3) (Van der Laan and Figueroa, 2014). XMCD exploits the difference in absorption of circularly polarized X-rays depending on the magnetization direction of the sample, enabling the detection of spin-resolved unoccupied electronic states through spin-orbit coupling. Conversely, XMLD uses linearly polarized X-rays to probe anisotropic charge distributions influenced by spin order, making it particularly useful for investigating antiferromagnetic and anisotropic ferromagnetic systems (Chen et al., 2019). These spectroscopic techniques can be extended into spatially resolved magnetic imaging using photoemission electron microscopy (PEEM) (Ohldag et al., 2009). In XMCD-PEEM and XMLD-PEEM, magnetic contrast arises from dichroic absorption differences, while the short wavelength of X-rays allows for nanoscale spatial resolution. This combination enables element-specific imaging of magnetic domains and domain walls. Overall, XMCD and XMLD, along with PEEM, provide powerful tools for understanding microscopic magnetic structures and spin configurations with high chemical and spatial resolution. This technique has been used to study a wide range of material systems, including thin films (Price et al., 2016), multilayers (Juge et al., 2022), and nanoparticles (Foerster et al., 2017). Additionally, XMLD and PEEM techniques offer unique advantages in observing antiferromagnetic moment reversal induced by spin-orbit torque (Ohldag et al., 2009; Wadley et al., 2016).

5 Conclusion and outlook

In this review, we systematically categorized magnetic measurement techniques into static, dynamic, and emerging classes. The static category, comprising VSM, AGM, SQUID magnetometer, MOKE microscope, and MFM, primarily addresses equilibrium magnetic properties. The dynamic category, including AC susceptometer and FMR-based systems, focuses on time- and frequency-dependent magnetization processes. In addition, we incorporated several emerging techniques originally developed for spintronic research, such as NV^- center magnetometry, SP-STM, LTEM, and soft X-ray-based techniques, which enable unprecedented exploration of spin structures and quantum-scale magnetic phenomena. For each technique, we primarily discussed its working principles and representative applications. These instruments demonstrate distinct strengths in specific measurement domains, from macroscopic hysteresis loop analysis and precise determination of magnetic parameters to nanoscale magnetic domain imaging. Collectively, they leverage a diverse array of physical mechanisms—including electromagnetic induction, quantum interference, magneto-optical effects, and scanning probe techniques, spin-dependent tunneling, spin-state readout—to form a multi-dimensional characterization matrix. In summary, Table 1 primarily highlights the spatial resolution, sample sensitivity, and main limitations of representative static and dynamic magnetic measurement techniques. Furthermore, Table 2 provides a comprehensive overview of all the techniques discussed, highlighting their applications and unique advantages in the field of spintronics.

In conclusion, magnetic measurement techniques have evolved into a diverse toolkit for probing magnetic materials across spatial, temporal, and energy scales. Building upon this foundation, future development is expected to follow several transformative directions that integrate advances in hardware, multi-physics coupling, intelligent data processing, and integrated on-chip sensing technologies. One prominent trajectory involves the development of high-field magnetic measurement platforms. Modern hybrid magnet systems are capable of generating ultrahigh magnetic fields that enable the exploration of novel magnetic phenomena beyond the reach of conventional instrumentation. For instance, the 45 T hybrid magnet developed at the High Magnetic Field Laboratory in Hefei, China, combines superconducting and resistive magnet technologies to provide a stable, user-accessible high-field environment (Bird, 2024). In parallel, pulsed-field systems reaching up to 100 T have been employed to probe exotic magnetic phases, such as field-induced quantum spin liquids in Kitaev materials (Zhou et al., 2023), highlighting the critical role of high magnetic fields in advancing quantum magnetism and emergent spin states.

TABLE 1 Summary of key performance parameters for static and dynamic magnetic measurement techniques. This table compares the selected techniques in terms of resolution (specifically referring to static magnetic moment resolution), measurement speed, sample sensitivity, operational cost, and limitations. The resolution and limitations of VSM are based on (Dodrill and Lindemuth, 2021); those of AGM refer to (Dodrill and Reichard, 2021); MOKE microscope data are from (McCord, 2015); and SQUID-related parameters are drawn from (Schmelz et al., 2016); the limitations of AC susceptometer are taken from (Topping and Blundell, 2018); and FMR-related performance indicators refer to (Mewes and Mewes, 2021).

Instruments	Resolution	Speed	Sample sensitivity	Operation costs	Limitations
VSM	10^{-7} emu	Fast	Bulk-sensitive	Low	Limited sensitivity
AGM	10^{-8} emu	Moderate	Bulk-sensitive	Low	Inaccurate characterization of soft magnetic materials
MOKE microscope	Non-quantitative	Fast	Surface-sensitive	Low	Limited penetration depth
MFM	—	Slow	Surface-sensitive	Moderate	Limited penetration depth
SQUID magnetometer	10^{-8} emu	Slow	Bulk-sensitive	High	The need for low-temperature
AC susceptometer	—	Slow	Bulk-sensitive	High	Limited frequency bandwidth
FMR-based system	—	Moderate	Bulk-sensitive	Low	Lack of spatial resolution

TABLE 2 Overview of magnetic measurement techniques and applications in spintronics. This table outlines the application domains and distinctive advantages of static, dynamic, and emerging techniques in spintronic research. It highlights the specific functions enabled by each method, such as domain imaging, magnetic hysteresis loop measurement, and related capabilities. The content of the table reflects and extends information already presented in the review, with relevant references as follows: VSM (Dodrill and Lindemuth, 2021); AGM (Dodrill and Reichard, 2021); SQUID magnetometer (Schmelz et al., 2016); MOKE microscope (Cao et al., 2024); MFM (Ghidini et al., 2022); NV^- center magnetometer (Zhang et al., 2025; Barry et al., 2020; Heitzer et al., 2024); SP-STM (Bagchi et al., 2024; Brüning et al., 2025); LTEM (Peng et., 2018; Xue, 2025); AC susceptometer (Borgohain and Borah, 2021; Fernández-García et al., 2022); FMR-based system (Coester et al., 2023; Zhan et al., 2024); and X-ray-based methods (Chen et al., 2019).

Instruments	Principle	Relevance to spintronics	Features
VSM	Electromagnetic induction	• Measuring magnetic hysteresis loops	• Compatible with diverse sample types • High stability; moderate sensitivity
AGM	Magnetic force balance	• Measuring hysteresis of spintronic samples	• Higher sensitivity than VSM
SQUID magnetometer	Superconductivity; Josephson effect	• Measuring ultra-weak magnetic moment • Detecting magnetic noise • Investigating quantum phenomena	• Exceptional sensitivity • Suitable for low-temperature and high-stability environments
MOKE microscope	MOKE	• Imaging magnetic domains • Probing magnetization reversal • Investigating spintronic device switching dynamics	• Spatial resolution of ~300 nm • Supports time-resolved studies (ps–ns) of fast magnetization dynamics
MFM	Measuring stray fields using a magnetic tip	• Imaging domain walls • Probing current-induced domain wall motion	• Moderate spatial resolution (tens of nanometers) • Sensitive to stray fields
NV– center magnetometer	Zeeman splitting with optical readout	• Imaging of domains and skyrmions • Probing antiferromagnetic and ferromagnetic spin textures • Detecting spin-wave dynamics and magnon modes	• Nanoscale resolution, no-invasive • Operable from room to cryogenic temperatures
SP-STM	Spin-dependent tunneling imaging	• Imaging spin textures (domain walls and skyrmions) • Probing local spin polarization and chiral spin configurations	• Atomic-scale spatial resolution, surface-sensitivity • Requires ultrahigh vacuum
LTEM	Lorentz deflection of electrons by internal magnetic fields	• Observing magnetic textures • Investigating topological spin structures	• High spatial resolution (2–20 nm) • Capable of dynamic in situ imaging
AC susceptometer	Mutual inductance	• Probing spin relaxation dynamics • Identifying spin-glass behavior • Characterizing magnetic phase transitions	• Sensitive to low-frequency magnetic dynamics • Supports variable frequency and temperature control
FMR-based system	Microwave excitation; resonant absorption	• Quantification of spin-orbit torque efficiency in spintronic devices • Measurement of damping constant and magnetic anisotropy	• Directly probes spin-orbit torque and damping • Highly sensitive to dynamic magnetic parameters
Soft X-ray-based techniques	Element- and spin-sensitive X-ray absorption	• Element-specific probing of magnetization in thin films and multilayers • Imaging of magnetic domains and spin textures	• High chemical and spatial resolution • Sensitivity to spin and orbital moments

A second important trend is the development of magneto-electric-optical multi-field coupling platforms that bridge the gap between macroscopic magnetic properties and microscopic magnetic structures. For example, molecule-based magnetic systems exemplify the progress in magnetic multi-field coupling, showcasing integrated optical, electronic, and magnetic responses such as magneto-chiral dichroism and opto-magneto-electric multifunctionality, with promising applications in quantum and sensing devices (Zakrzewski et al., 2024).

The third direction lies in the integration of artificial intelligence (AI) into magnetic measurement workflows. AI-driven platforms are enabling closed-loop pipelines encompassing data acquisition, real-time analysis, and decision feedback. For instance, Talapatra et al. (2023) trained a convolutional neural network (CNN) on simulated magnetic domain images to predict key micromagnetic parameters with accuracies up to 93.9%, while McCray et al. (2024) developed a machine learning model that automatically identifies and quantifies magnetic skyrmions from LTEM images with 97.6% accuracy in position detection. These examples underscore how machine learning not only accelerates data analysis but also enables intelligent interpretation of complex magnetic textures.

Beyond these trends, the advancement of integrated on-chip magnetometers represents another key trajectory. Recent progress in NV center, atomic, and solid-state magnetometry has shown the feasibility of achieving high sensitivity and spatial resolution within compact, CMOS-compatible platforms. These miniaturized systems significantly reduce hardware complexity while enabling multi-channel detection of magnetic fields at the microscale. As photonic integration, quantum sensing, and advanced microfabrication technologies continue to mature, chip-scale magnetometers are expected to evolve into scalable, low-power, and application-specific solutions. This evolution will accelerate the deployment of magnetic sensing technologies into diverse applications such as biomedical diagnostics, microscale magnetic imaging, and quantum information processing. Enabled by atomic-scale detection mechanisms, emerging quantum magnetic sensors—such as SQUIDs, NV centers, and atomic magnetometers—offer unprecedented precision, paving the way for a new era of magnetic metrology.

This evolution, driven by synergistic advancements in high-field instrumentation, multi-field coupling, AI algorithm integration, and on-chip sensing technologies, is transforming magnetic measurement from a set of passive diagnostic tools into intelligent, scalable platforms for scientific discovery. Such progress is expected to continuously propel breakthroughs in spintronics, quantum magnetism, and energy-related materials, while expanding the role of magnetic characterization in both fundamental research and emerging real-world applications.

Author contributions

JZ: Conceptualization, Methodology, Writing – original draft. LB: Conceptualization, Methodology, Writing – original draft. SL: Formal Analysis, Writing – review and editing. ZC: Funding acquisition, Supervision, Writing – review and editing. YP: Visualization, Writing – review and editing. JB: Investigation, Validation, Writing – original draft. XC: Project administration, Resources, Software, Writing – original draft. XS: Data curation, Visualization, Writing – review and editing. XL: Visualization, Writing – review and editing. GW: Funding acquisition, Supervision, Writing – review and editing. XZ: Funding acquisition, Supervision, Writing – review and editing.

Funding

The author(s) declare that financial support was received for the research and/or publication of this article. This work was supported by the Key R&D Plan of Shandong Province (2022CXGC020208), Beijing Municipal Natural Science Foundation (Z230004), the National Natural Science Foundation of China (52261145,694, 92164206, W2411060, 12404118), and China Postdoctoral Science Foundation (2024M754047, GZC20242163).

Conflict of interest

Authors ZC and XZ were employed by Truth Instruments Co. Ltd.

The remaining authors declare that the research was conducted in the absence of any commercial or financial relationships that could be construed as a potential conflict of interest.

Generative AI statement

The author(s) declare that no Generative AI was used in the creation of this manuscript.

Publisher's note

References

Adam, J. P., Rohart, S., Jamet, J. P., Mougin, A., Ferré, J., Bernas, H., et al. (2009). Single Pt/Co (0.5 nm)/Pt nano-discs: beyond the coherent spin reversal model and thermal stability. *J. Magnetics Soc. Jpn.* 33 (6_2), 498–502. doi:10.3379/msjmag.0907MI0009

Adam, J., Jamet, J., Ferré, J., Mougin, A., Rohart, S., Weil, R., et al. (2010). Magnetization reversal in Pt/Co (0.5 nm)/Pt nano-platelets patterned by focused ion beamlithography. *Nanotechnology* 21 (44), 445302. doi:10.1088/0957-4484/21/44/445302

Adanlété Adjanoh, A., Pakam, T., and Afenyiveh, S. D. M. (2024). Magnetic domain and structural defects size in ultrathin films. *Phys. Status Solidi – Rapid Res. Lett.* 19 (1), 2400215. doi:10.1002/pssr.202400215

Amir, M., Mishra, V., Sharma, R., Iqbal, F., Ali, S. W., Kumar, S., et al. (2023). Development of magnetic nanoparticle based nanoabrasives for magnetorheological finishing process and all their variants. *Ceram. Int.* 49 (4), 6254–6261. doi:10.1016/j.ceramint.2022.11.033

Anbuselvan, D., Nilavazhagan, S., Santhanam, A., Chidhambaram, N., Gunavathy, K. V., Ahamad, T., et al. (2021). Room temperature ferromagnetic behavior of nickel-doped zinc oxide dilute magnetic semiconductor for spintronics applications. *Phys. E Low-Dimensional Syst. Nanostructures* 129, 114665. doi:10.1016/j.physe.2021.114665

Argyres, P. N. (1955). Theory of the Faraday and Kerr effects in ferromagnetics. *Phys. Rev.* 97 (2), 334–345. doi:10.1103/PhysRev.97.334

Bagchi, M., Tounsi, T. Y., Safeer, A., Efferen, C. V., Rosch, A., Michely, T., et al. (2024). Spin-polarized scanning tunneling microscopy measurements of an Anderson impurity. *Phys. Rev. Lett.* 133 (24), 246701. doi:10.1103/PhysRevLett.133.246701

Bałanda, M. (2013). AC susceptibility studies of phase transitions and magnetic relaxation: conventional, molecular and low-dimensional magnets. *Acta Phys. Pol. A* 124 (6), 964–976. doi:10.12693/APhysPolA.124.964

Barbic, M. (2004). Sensitive measurement of reversible parallel and transverse susceptibility by alternating gradient magnetometry. *Rev. Sci. Instrum.* 75 (11), 5016–5021. doi:10.1063/1.1808096

Barry, J. F., Schloss, J. M., Bauch, E., Turner, M. J., Hart, C. A., Pham, L. M., et al. (2020). Sensitivity optimization for NV^- diamond magnetometry. *Rev. Mod. Phys.* 92, 015004. doi:10.1103/RevModPhys.92.015004

Béa, H., Gajek, M., Bibes, M., and Barthélémy, A. (2008). Spintronics with multiferroics. *J. Phys. Condens. Matter* 20 (43), 11. doi:10.1088/0953-8984/20/43/434221

Beik Mohammadi, J., Jones, J. M., Paul, S., Khodadadi, B., Mewes, C. K., Mewes, T., et al. (2017). Broadband ferromagnetic resonance characterization of anisotropies and relaxation in exchange-biased IrMn/CoFe bilayers. *Phys. Rev. B* 95 (6), 064414. doi:10.1103/PhysRevB.95.064414

Beik Mohammadi, J., Mankey, G., Mewes, C. K., and Mewes, T. (2019). Strong interfacial perpendicular anisotropy and interfacial damping in $Ni_{0.8}Fe_{0.2}$ films adjacent to Ru and SiO_2. *J. Appl. Phys.* 125 (2), 023901. doi:10.1063/1.5052334

Bhattacharjee, N., Sapozhnik, A. A., Bodnar, S. Y., Grigorev, V. Y., Agustsson, S. Y., Cao, J., et al. (2018). Néel spin-orbit torque driven antiferromagnetic resonance in Mn_2Au probed by time-domain THz spectroscopy. *Phys. Rev. Lett.* 120 (23), 237201. doi:10.1103/PhysRevLett.120.237201

Bird, M. D. (2024). Superconducting magnet technology for the outer coils of resistive -superconducting hybrid magnets. *Supercond. Sci. Technol.* 37 (12), 123003. doi:10.1088/1361-6668/ad8af0

Blundell, S. (2001). *Magnetism in condensed matter*. Oxford: OUP.

Bode, M. (2003). Spin-polarized scanning tunnelling microscopy. *Rep. Prog. Phys.* 66 (4), 523–582. doi:10.1088/0034-4885/66/4/203

Borgohain, C., and Borah, J. P. (2021). A versatile and cost-effective automation of an AC susceptometer using Virtual Instruments and Arduino-Uno microcontroller. *J. Instrum.* 16 (10), P10028. doi:10.1088/1748-0221/16/10/P10028

Bouchiat, V. (2009). Detection of magnetic moments using a nano-SQUID: limits of resolution and sensitivity innear-field SQUID magnetometry. *Supercond. Sci. Technol.* 22 (6), 064002. doi:10.1088/0953-2048/22/6/064002

Brüning, R., Rózsa, L., Lo Conte, R., Kubetzka, A., Wiesendanger, R., and von Bergmann, K. (2025). Topological meron-antimeron domain walls and skyrmions in a low-symmetry system. *Phys. Rev. X* 15 (2), 021041. doi:10.1103/PhysRevX.15.021041

Bruno, P., Suzuki, Y., and Chappert, C. (1996). Magneto-optical Kerr effect in a paramagnetic overlayer on a ferromagnetic substrate: a spin-polarized quantum size effect. *Phys. Rev. B* 53 (14), 9214–9220. doi:10.1103/PhysRevB.53.9214

Buchner, M., Höfler, K., Henne, B., Ney, V., and Ney, A. (2018). Tutorial: basic principles, limits of detection, and pitfalls of highly sensitive SQUID magnetometry for nanomagnetism and spintronics. *J. Appl. Phys.* 124 (16), 161101. doi:10.1063/1.5045299

Burn, D., Zhang, S., Van der Laan, G., and Hesjedal, T. (2021). Magnetization dynamics in ordered spin structures revealed by diffractive and reflectometry ferromagnetic resonance. *AIP Adv.* 11 (1), 015327. doi:10.1063/9.0000058

Cafolla-Ward, C. (2024). *Using High Frequency A. C. Susceptibility to Probe Frustrated Magnetic Systems.* PhD Thesis, Wales: Cardiff University. Available online at: https://orca.cardiff.ac.uk/id/eprint/172700

Cao, Z., Li, S., Pan, Y., Zhao, J., Ye, S., Zhang, X., et al. (2024). Characterization of magnetic thin films and spintronic devices using magneto-optic Kerr microscopy. *Adv. Devices Instrum.* 5, 0060. doi:10.34133/adi.0060

Casimir, H., and Du Pré, F. (1938). Note on the thermodynamic interpretation of paramagnetic relaxation phenomena. *Physica* 5 (6), 507–511. doi:10.1016/S0031-8914(38)80164-6

Celik, H., Kannan, H., Wang, T., Mellnik, A., Fan, X., Zhou, X., et al. (2019). Vector-resolved magnetooptic Kerr effect measurements of spin-orbit torque. *IEEE Trans. Magnetics* 55 (1), 1–5. doi:10.1109/TMAG.2018.2873129

Chen, X., Zhou, X., Cheng, R., Song, C., Zhang, J., Wu, Y., et al. (2019). Electric field control of Néel spin–orbit torque in an antiferromagnet. *Nat. Mater.* 18, 931–935. doi:10.1038/s41563-019-0424-2

Chen, T., Peng, C., Liao, W., and Pai, C. (2021). Characterization of spin-orbit torque efficiency in the RF regime for MRAM applications. in *2021 IEEE International Symposium on Radio-Frequency* Integration Technology (RFIT). New Jersey: IEEE. doi:10.1109/RFIT52905.2021.9565262

Chen, Z., Turgut, E., Jiang, Y., Nguyen, K. X., Stolt, M. J., Jin, S., et al. (2022). Lorentz electron ptychography for imaging magnetic textures beyond the diffraction limit. *Nat. Nanotechnol.* 17, 1165–1170. doi:10.1038/s41565-022-01224-y

Chen, S., Lourembam, J., Ho, P., Toh, A. K. J., Huang, J., Chen, X., et al. (2024). All-electrical skyrmionic magnetic tunnel junction. *Nature* 627 (8004), 522–527. doi:10.1038/s41586-024-07131-7

Ciprian, R., Loi, F., Busetto, E., Bonanni, V., Casarin, B., Caretta, A., et al. (2018). MOKE setup exploiting a nematic liquid crystal modulator. *Rev. Sci. Instrum.* 89 (10), 105107. doi:10.1063/1.5033433

Coester, B., Lim, G. J., Tan, F. N., Poh, H. Y., and Lew, W. S. (2023). Investigation of spin-orbit torque performance with W/Cu-multilayers as spin current source. *J. Appl. Phys.* 133 (22), 223904. doi:10.1063/5.0139212

Corbett, J. P., Meng, K. Y., Repicky, J. J., Garcia-Diaz, R., Rowland, J. R., Ahmed, A. S., et al. (2022). Spin polarized STM imaging of nanoscale Néel Skyrmions in an $SrIrO_3$/$SrRuO_3$ perovskite bilayer. *Appl. Surf. Sci.* 599, 153766. doi:10.1016/j.apsusc.2022.153766

Cullity, B. D., and Graham, C. D. (2011). *Introduction to magnetic materials*. New Jersey: John Wiley and Sons.

Dai, H., Hafner, J. H., Rinzler, A. G., Colbert, D. T., and Smalley, R. E. (1996). Nanotubes as nanoprobes in scanning probe microscopy. *Nature* 384 (6605), 147–150. doi:10.1038/384147a0

Demidov, V. E., Urazhdin, S., and Demokritov, S. O. (2010). Direct observation and mapping of spin waves emitted by spin-torque nano-oscillators. *Nat. Mater.* 9 (12), 984–988. doi:10.1038/nmat2882

Demidov, V., Urazhdin, S., Edwards, E., and Demokritov, S. (2011). Wide-range control of ferromagnetic resonance by spin Hall effect. *Appl. Phys. Lett.* 99 (17), 172501. doi:10.1063/1.3655908

Ding, H., Putter, S., Oepen, H., and Kirschner, J. (2000). Experimental method for separating longitudinal and polar Kerr signals. *J. Magnetism Magnetic Mater.* 212, 5–11. doi:10.1016/S0304-8853(99)00790-8

Ding, H. F., Pütter, S., Oepen, H. P., and Kirschner, J. (2001). Spin-reorientation transition in thin films studied by the component-resolved Kerr effect. *Phys. Rev. B* 63 (13), 134425. doi:10.1103/PhysRevB.63.134425

Doaga, A., Cojocariu, A., Constantin, C., Hempelmann, R., and Caltun, O. (2013). "Magnetic nanoparticles for medical applications: progress and challenges," in *AIP conference proceedings*. New York: American Institute of Physics, 123–131.

Dodrill, B., and Lindemuth, J. R. (2021). "Vibrating sample magnetometry," in *Magnetic measurement techniques for materials characterization*. Editors V. Franco, and B. Dodrill (Cham: Springer International Publishing), 15–37.

Dodrill, B., and Reichard, H. S. (2021). "Alternating gradient magnetometry," in *Magnetic measurement techniques for materials characterization*. Editors V. Franco, and B. Dodrill (Cham: Springer International Publishing), 139–149.

Domenichini, P., Quinteros, C. P., Granada, M., Collin, S., George, J.-M., Curiale, J., et al. (2019). Transient magnetic-domain-wall ac dynamics by means of magneto-optical Kerr effect microscopy. *Phys. Rev. B* 99 (21), 214401. doi:10.1103/PhysRevB.99.214401

Dorfmann, J. (1923). Einige bemerkungen zur kenntnis des mechanismus magnetischer erscheinungen. *Z. für Phys.* 17 (1), 98–111. doi:10.1007/BF01328670

Dovzhenko, Y., Casola, F., Schlotter, S., Zhou, T. X., Buttner, F., Walsworth, R. L., et al. (2018). Magnetostatic twists in room-temperature skyrmions explored by nitrogen-vacancy center spin texture reconstruction. *Nat. Commun.* 9, 2712. doi:10.1038/s41467-018-05158-9

Dumas, R. K., and Hogan, T. (2021). "Recent advances in SQUID magnetometry," in *Magnetic measurement techniques for MaterialsCharacterization*. Editors V. Franco, and B. Dodrill (Cham: Springer International Publishing), 39–62.

Edgar, A., and Quilty, J. (1993). A mutual inductance apparatus for measuring magnetic susceptibility and electrical conductivity. *Am. J. Phys.* 61 (10), 943–946. doi:10.1119/1.17373

El-Alaily, T. M., El-Nimr, M. K., Saafan, S. A., Kamel, M. M., Meaz, T. M., and Assar, S. T. (2015). Construction and calibration of a low cost and fully automated vibrating sample magnetometer. *J. Magnetism Magnetic Mater.* 386, 25–30. doi:10.1016/j.jmmm.2015.03.051

El-Bassuony, A. A. H., and Abdelsalam, H. K. (2017). Giant exchange bias of hysteresis loops on Cr^{3+}-doped Ag nanoparticles. *J. Supercond. Nov. Magnetism* 31 (5), 1539–1544. doi:10.1007/s10948-017-4340-x

Erlandsson, R., McClelland, G., Mate, C., and Chiang, S. (1988). Atomic force microscopy using optical interferometry. *J. Vac. Sci. Technol. A* 6 (2), 266–270. doi:10.1116/1.575440

Fagaly, R. L. (2006). Superconducting quantum interference device instruments and applications. *Rev. Sci. Instrum.* 77 (10), 101101. doi:10.1063/1.2354545

Feng, Y., Mandru, A. O., Yıldırım, O., and Hug, H. J. (2022a). Quantitative magnetic force microscopy: transfer-function method revisited. *Phys. Rev. Appl.* 18 (2), 024016. doi:10.1103/PhysRevApplied.18.024016

Feng, Y., Vaghefi, P. M., Vranjkovic, S., Penedo, M., Kappenberger, P., Schwenk, J., et al. (2022b). Magnetic force microscopy contrast formation and field sensitivity. *J. Magnetism Magnetic Mater.* 551, 169073. doi:10.1016/j.jmmm.2022.169073

Feng, X., Zhai, B., Cheng, R., Yin, L., Wen, Y., Jiang, J., et al. (2023). Phase engineering of 2D spinel-type manganese oxides. *Adv. Mater.* 35 (42), 2304118. doi:10.1002/adma.202304118

Fernández-García, M. P., Teixeira, J. M., González, dlV. M., Moreira, J. C., and Araújo, J. P. (2022). Delving into the aqueous coprecipitation synthesis of Fe-oxide nanoparticles with a real time AC susceptometer. *Appl. Phys. A* 128 (3), 209. doi:10.1007/s00339-022-05342-1

Flanders, P. J. (1988). An alternating-gradient magnetometer (invited). *J. Appl. Phys.* 63 (8), 3940–3945. doi:10.1063/1.340582

Flanders, P. J. (1990). A vertical force alternating-gradient magnetometer. *Rev. Sci. Instrum.* 61 (2), 839–847. doi:10.1063/1.1141451

Foerster, M., Macià, F., Statuto, N., Finizio, S., Hernández-Mínguez, A., Lendínez, S., et al. (2017). Direct imaging of delayed magneto-dynamic modes induced by surface acoustic waves. *Nat. Commun.* 8 (1), 407. doi:10.1038/s41467-017-00456-0

Foner, S. (1956). Vibrating sample magnetometer. *Rev. Sci. Instrum.* 27 (7), 548. doi:10.1063/1.1715636

Foner, S. (1959). Versatile and sensitive vibrating-sample magnetometer. *Rev. Sci. Instrum.* 30 (7), 548–557. doi:10.1063/1.1716679

Foner, S. (1996). The vibrating sample magnetometer: experiences of a volunteer (invited). *J. Appl. Phys.* 79 (8), 4740–4745. doi:10.1063/1.361657

Franco, V., and Dodrill, B. (2021). *Magnetic measurement techniques for materials characterization*. Cham: Springer.

Frandsen, B. A., Read, C., Stevens, J., Walker, C., Christiansen, M., Harrison, R. G., et al. (2021). Superparamagnetic dynamics and blocking transition in Fe_3O_4 nanoparticles probed by vibrating sample magnetometry and muon spin relaxation. *Phys. Rev. Mater.* 5 (5), 054411. doi:10.1103/PhysRevMaterials.5.054411

Freitag, N. H., Reiche, C. F., Neu, V., Devi, P., Burkhardt, U., Felser, C., et al. (2023). Simultaneous magnetic field and field gradient mapping of hexagonal MnNiGa by quantitative magnetic force microscopy. *Commun. Phys.* 6 (1), 11. doi:10.1038/s42005-022-01119-3

Frey, T., Jantz, W., and Stibal, R. (1988). Compensating vibrating reed magnetometer (invited). *J. Appl. Phys.* 64 (10), 6002–6007. doi:10.1063/1.342132

Gatteschi, D., Sessoli, R., and Villain, J. (2006). *Molecular nanomagnets*. Oxford: Oxford University Press.

Ghidini, M., Maccherozzi, F., Dhesi, S., and Mathur, N. (2022). XPEEM and MFM imaging of ferroic materials. *Adv. Electron. Mater.* 8 (6), 2200162. doi:10.1002/aelm.202200162

Ghigo, G., Fracasso, M., Gerbaldo, R., Gozzelino, L., Laviano, F., Napolitano, A., et al. (2022). High-frequency ac susceptibility of iron-based superconductors. *Materials* 15 (3), 1079. doi:10.3390/ma15031079

Göddenhenrich, T., Hartmann, U., Anders, M., and Heiden, C. (1988). Investigation of Bloch wall fine structures by magnetic force microscopy. *J. Microsc.* 152 (2), 527–536. doi:10.1111/j.1365-2818.1988.tb01417.x

Godsell, J. F., Kulkarni, S., O'Donnell, T., and Roy, S. (2010). Precessional dynamics of $Ni_{45}Fe_{55}$ thin films for ultrahigh frequency integrated magnetics. *J. Appl. Phys.* 107 (3), 033907. doi:10.1063/1.3276165

Gömöry, F. (1997). Characterization of high-temperature superconductors by AC susceptibility measurements. *Supercond. Sci. Technol.* 10 (8), 523–542. doi:10.1088/0953-2048/10/8/001

Greening, R. W., DeVisscher, E. D., and Fan, X. (2025). A method to suppress polar Kerr signal in a longitudinal magneto-optic-Kerr-effect measurement. *IEEE Magn. Lett.* 16, 8100205. doi:10.1109/LMAG.2025.3577473

Griffiths, J. H. (1946). Anomalous high-frequency resistance of ferromagnetic metals. *Nature* 158 (4019), 670–671. doi:10.1038/158670a0

Grinolds, M. S., Hong, S., Maletinsky, P., Luan, L., Lukin, M. D., Walsworth, R. L., et al. (2013). Nanoscale magnetic imaging of a single electron spin under ambient conditions. *Nat. Phys.* 9, 215–219. doi:10.1038/nphys2543

Grinolds, M. S., Warner, M., De Greve, K., Dovzhenko, Y., Thiel, L., Walsworth, R. L., et al. (2014). Subnanometre resolution in three-dimensional magnetic resonance imaging of individual dark spins. *Nat. Nanotechnol.* 9, 279–284. doi:10.1038/nnano.2014.30

Grundy, P. J., and Tebble, R. S. (1968). Lorentz electron microscopy. *Adv. Phys.* 17 (66), 153–242. doi:10.1080/00018736800101286

Guo, S. (2023). An overview of NV centers. *J. Appl. Math. Phys.* 11 (11), 3666–3675. doi:10.4236/jamp.2023.1111231

Guo, Z., Wang, J., Malinowski, G., Zhang, B., Zhang, W., Wang, H., et al. (2024). Single-shot laser-induced switching of an exchange biased antiferromagnet. *Adv. Mater.* 36 (21), 2311643. doi:10.1002/adma.202311643

Hale, M. E., Fuller, H. W., and Rubenstein, H. (1959). Magnetic domain observations by electron microscopy. *J. Appl. Phys.* 30, 789–791. doi:10.1063/1.1735233

Han, G., Wu, Y., and Zheng, Y. (2007). Double exchange biased magnetic force microscopy tip and comparison of its imaging performance with commercial tips. *Jpn. J. Appl. Phys.* 46 (7R), 4403. doi:10.1143/JJAP.46.4403

Hartmann, U. (1999). Magnetic force microscopy. *Annu. Rev. Mater. Res.* 29 (1), 53–87. doi:10.1146/annurev.matsci.29.1.53

Hartshorn, L. (1925). A precision method for the comparison of unequal mutual inductances at telephonic frequencies. *J. Sci. Instrum.* 2 (5), 145–151. doi:10.1088/0950-7671/2/5/301

Hassdenteufel, A., Hebler, B., Schubert, C., Liebig, A., Teich, M., Helm, M., et al. (2013). Thermally assisted all-optical helicity dependent magnetic switching in amorphous $Fe_{100-x}Tb_x$ alloy films. *Adv. Mater.* 25 (22), 3122–3128. doi:10.1002/adma.201300176

Heitzer, R. C., Pinto, F., Rodríguez, E., Rodríguez-Suárez, R., and Maze, J. R. (2024). Characterization of antiferromagnetic magnons using nitrogen vacancy center relaxometry. *Phys. Rev. B* 110 (13), 134431. doi:10.1103/PhysRevB.110.134431

Henrichs, L. F., Cespedes, O., Bennett, J., Landers, J., Salamon, S., Heuser, C., et al. (2016). Multiferroic clusters: a new perspective for relaxor-type room-temperature multiferroics. *Adv. Funct. Mater.* 26, 2111–2121. doi:10.1002/adfm.201503335

Hibino, Y., Taniguchi, T., Yakushiji, K., Kubota, H., and Yuasa, S. (2024). Observation of self-induced spin-orbit torques in Ni-Fe layers with a vertical gradient of magnetization. *Phys. Rev. B* 109 (18), L180409. doi:10.1103/PhysRevB.109.L180409

Hill, E. W., Nazran, P., and Tailor, P. (1996). A versatile vibrating reed and magneto-optic magnetometer. *IEEE Trans. Magnetics* 32 (5), 4899–4901. doi:10.1109/20.539281

Hong, S., Grinolds, M. S., Pham, L. M., Le Sage, D., Luan, L., Walsworth, R. L., et al. (2013). Nanoscale magnetometry with NV centers in diamond. *MRS Bull.* 38 (2), 155–161. doi:10.1557/mrs.2013.23

Hrabec, A., Porter, N., Wells, A., Benitez, M., Burnell, G., McVitie, S., et al. (2014). Measuring and tailoring the Dzyaloshinskii-Moriya interaction in perpendicularly magnetized thin films. *Phys. Rev. B* 90 (2), 020402. doi:10.1103/physrevb.90.020402

Hurt, D., Li, S., and Amann, A. (2013). Versatile SQUID susceptometer with multiple measurement modes. *IEEE Trans. Magnetics* 49 (7), 3541–3544. doi:10.1109/TMAG.2013.2241029

Igarashi, J., Zhang, W., Remy, Q., Díaz, E., Lin, J. X., Hohlfeld, J., et al. (2023). Optically induced ultrafast magnetization switching in ferromagnetic spin valves. *Nat. Mater.* 22 (6), 725–730. doi:10.1038/s41563-023-01499-z

Igarashi, J., Le Guen, Y., Hohlfeld, J., Mangin, S., Gorchon, J., Hehn, M., et al. (2024). Influence of interlayer exchange coupling on ultrafast laser-induced magnetization reversal in ferromagnetic spin valves. *Phys. Rev. B* 109 (9), 094422. doi:10.1103/PhysRevB.109.094422

Jabbar, R., Sabeeh, S. H., and Hameed, A. M. (2020). Structural, dielectric and magnetic properties of Mn^{+2} doped cobalt ferrite nanoparticles. *J. Magnetism Magnetic Mater.* 494, 165726. doi:10.1016/j.jmmm.2019.165726

Jordán, D., González-Chávez, D., Laura, D., León Hilario, L. M., Monteblanco, E., Gutarra, A., et al. (2018). Detection of magnetic moment in thin films with a home-made vibrating sample magnetometer. *J. Magnetism Magnetic Mater.* 456, 56–61. doi:10.1016/j.jmmm.2018.01.088

Juge, R., Sisodia, N., Larrañaga, J. U., Zhang, Q., Pham, V. T., Rana, K. G., et al. (2022). Skyrmions in synthetic antiferromagnets and their nucleation via electrical current and ultra-fast laser illumination. *Nat. Commun.* 13 (1), 4807. doi:10.1038/s41467-022-32525-4

Jumpertz, R., Leinenbach, P., Van der Hart, A., and Schelten, J. (1997). Magnetically refined tips for scanning force microscopy. *Microelectron. Eng.* 35 (1-4), 325–328. doi:10.1016/S0167-9317(96)00133-5

Kalarickal, S. S., Krivosik, P., Wu, M., Patton, C. E., Schneider, M. L., Kabos, P., et al. (2006). Ferromagnetic resonance linewidth in metallic thin films: comparison of measurement methods. *J. Appl. Phys.* 99 (9), 093909. doi:10.1063/1.2197087

Kato, Y. D., Okamura, Y., Hirschberger, M., Tokura, Y., and Takahashi, Y. (2023). Topological magneto-optical effect from skyrmion lattice. *Nat. Commun.* 14 (1), 5416. doi:10.1038/s41467-023-41203-y

Kazakova, O., Puttock, R., Barton, C., Corte-León, H., Jaafar, M., Neu, V., et al. (2019). Frontiers of magnetic force microscopy. *J. Appl. Phys.* 125 (6), 060901. doi:10.1063/1.5050712

Ke, W.-E., Shao, P.-W., Kuo, C.-Y., Song, H., Huang, R., Yagi, N., et al. (2021). Barium hexaferrite/muscovite heteroepitaxy with mechanically robust perpendicular magnetic anisotropy. *npj Flex. Electron.* 5 (1), 33. doi:10.1038/s41528-021-00130-y

Kennewell, K., Kostylev, M., Ross, N., Magaraggia, R., Stamps, R., Ali, M., et al. (2010). Magnetization pinning at a Py/Co interface measured using broadband inductive magnetometry. *J. Appl. Phys.* 108 (7), 073917. doi:10.1063/1.3488618

Kermanian, M., Naghibi, M., and Sadighian, S. (2020). One-pot hydrothermal synthesis of a magnetic hydroxyapatite nanocomposite for MR imaging and pH-Sensitive drug delivery applications. *Heliyon* 6 (9), e04928. doi:10.1016/j.heliyon.2020.e04928

Kerr, J. J. T. L., Magazine, D. P., and Science, J. o. (1877). XLIII. On rotation of the plane of polarization by reflection from the pole of a magnet. *Lond. Edinb. Dublin Philosophical Mag. J. Sci.* 3 (19), 321–343. doi:10.1080/14786447708639245

Khodadadi, B., Rai, A., Sapkota, A., Srivastava, A., Nepal, B., Lim, Y., et al. (2020). Conductivitylike Gilbert damping due to intraband scattering in epitaxial iron. *Phys. Rev. Lett.* 124 (15), 157201. doi:10.1103/physrevlett.124.157201

Kim, S. J., Lee, D. K., Oh, S. H., Koo, H. C., and Lee, K. J. (2021). Theory of spin-torque ferrimagnetic resonance. *Phys. Rev. B* 104 (2), 024405. doi:10.1103/PhysRevB.104.024405

Kirilyuk, A., Kimel, A. V., and Rasing, T. (2010). Ultrafast optical manipulation of magnetic order. *Rev. Mod. Phys.* 82 (3), 2731–2784. doi:10.1103/RevModPhys.82.2731

Kirtley, J., Ketchen, M., Stawiasz, K., Sun, J., Gallagher, W., Blanton, S., et al. (1995). High-resolution scanning SQUID microscope. *Appl. Phys. Lett.* 66 (9), 1138–1140. doi:10.1063/1.113838

Kiselev, S. I., Sankey, J., Krivorotov, I., Emley, N., Schoelkopf, R., Buhrman, R., et al. (2003). Microwave oscillations of a nanomagnet driven by a spin-polarized current. *Nature* 425 (6956), 380–383. doi:10.1038/nature01967

Kittel, C. (1948). On the theory of ferromagnetic resonance absorption. *Phys. Rev.* 73 (2), 155–161. doi:10.1103/PhysRev.73.155

Kotani, A., Nakajima, H., Harada, K., Ishii, Y., and Mori, S. (2016). Lorentz microscopy and small-angle electron diffraction study of magnetic textures in $La_{1-x}Sr_xMnO_3$ ($0.15 < x < 0.30$): the role of magnetic anisotropy. *Phys. Rev. B* 94 (2), 024407. doi:10.1103/physrevb.94.024407

Krivcov, A., Junkers, T., and Möbius, H. (2018). Understanding electrostatic and magnetic forces in magnetic force microscopy: towards single superparamagnetic nanoparticle resolution. *J. Phys. Commun.* 2 (7), 075019. doi:10.1088/2399-6528/aad3a4

Lah, N. A. C., Mesran, M. N., and Saari, M. M. (2020). Frequency-dependent of AC susceptibility in chitosan oligosaccharide-Ag nanostructures. *J. Alloys Compd.* 835, 155366. doi:10.1016/j.jallcom.2020.155366

Lalieu, M. L. M., Peeters, M. J. G., Haenen, S. R. R., Lavrijsen, R., and Koopmans, B. (2017). Deterministic all-optical switching of synthetic ferrimagnets using single femtosecond laser pulses. *Phys. Rev. B* 96 (22), 220411. doi:10.1103/PhysRevB.96.220411

Lalieu, M. L. M., Lavrijsen, R., and Koopmans, B. (2019). Integrating all-optical switching with spintronics. *Nat. Commun.* 10 (1), 110. doi:10.1038/s41467-018-08062-4

Landau, L., and Lifshitz, E. (1935). On the theory of the dispersion of magnetic permeability in ferromagnetic bodies. *Phys. Z. Sowjetunion* 8, 153–169. doi:10.1016/B978-0-08-036364-6.50008-9

Lavrijsen, R., Lee, J. H., Fernandez-Pacheco, A., Petit, D. C., Mansell, R., and Cowburn, R. P. (2013). Magnetic ratchet for three-dimensional spintronic memory and logic. *Nature* 493 (7434), 647–650. doi:10.1038/nature11733

Lee, H., Wang, Y. H., Mewes, C., Butler, W., Mewes, T., Maat, S., et al. (2009). Magnetization relaxation and structure of CoFeGe alloys. *Appl. Phys. Lett.* 95 (8), 082502. doi:10.1063/1.3207749

Lee, S. H., Kim, Y., Cho, B., Park, J., Kim, M. S., Park, K., et al. (2022). Spin-polarized and possible pseudospin-polarized scanning tunneling microscopy in kagome metal FeSn. *Commun. Phys.* 5 (1), 235. doi:10.1038/s42005-022-01012-z

Lesik, M., Plisson, T., Toraille, L., Renaud, J., Occelli, F., Schmidt, M., et al. (2019). Magnetic measurements on micrometer-sized samples under high pressure using designed NV centers. *Science* 366, 1359–1362. doi:10.1126/science.aaw4329

Liu, Z., Dan, Y., Jinjun, Q., and Wu, Y. (2002). Magnetic force microscopy using focused ion beam sharpened tip with deposited antiferro-ferromagnetic multiple layers. *J. Appl. Phys.* 91 (10), 8843–8845. doi:10.1063/1.1456056

Liu, G., Feng, X., Wang, N., Li, Q., and Liu, R. (2019). Coherent quantum control of nitrogen-vacancy center spins near 1000 kelvin. *Nat. Commun.* 10, 1344. doi:10.1038/s41467-019-09327-2

Lopez-Dominguez, V., Quesada, A., Guzman-Minguez, J. C., Moreno, L., Lere, M., Spottorno, J., et al. (2018). A simple vibrating sample magnetometer for macroscopic samples. *Rev. Sci. Instrum.* 89 (3), 034707. doi:10.1063/1.5017708

Magni, A., Carlotti, G., Casiraghi, A., Darwin, E., Durin, G., Diez, L. H., et al. (2022). Key points in the determination of the interfacial Dzyaloshinskii–Moriya interaction from asymmetric bubble domain expansion. *IEEE Trans. Magnetics* 58 (12), 1–16. doi:10.1109/TMAG.2022.3217891

Mallick, S., Sassi, Y., Prestes, N. F., Krishnia, S., Gallego, F., Vicente Arche, L. M., et al. (2024). Driving skyrmions in flow regime in synthetic ferrimagnets. *Nat. Commun.* 15 (1), 8472. doi:10.1038/s41467-024-52210-y

Mallinson, J. (1966). Magnetometer coils and reciprocity. *J. Appl. Phys.* 37, 2514–2515. doi:10.1063/1.1708848

Marschall, M., Sievers, S., Schumacher, H. W., and Elster, C. (2022). Uncertainty propagation in quantitative magnetic force microscopy using a Monte-Carlo method. *IEEE Trans. Magnetics* 58 (5), 1–8. doi:10.1109/TMAG.2022.3153176

Martin, Y., Williams, C. C., and Wickramasinghe, H. K. (1987). Atomic force microscope–force mapping and profiling on a sub 100-Å scale. *J. Appl. Phys.* 61 (10), 4723–4729. doi:10.1063/1.338807

Maze, J. R., Stanwix, P. L., Hodges, J. S., Hong, S., Taylor, J. M., Cappellaro, P., et al. (2008). Nanoscale magnetic sensing with an individual electronic spin in diamond. *Nature* 455, 644–647. doi:10.1038/nature07279

McCord, J. (2015). Progress in magnetic domain observation by advanced magneto-optical microscopy. *J. Phys. D Appl. Phys.* 48 (33), 333001. doi:10.1088/0022-3727/48/33/333001

McCray, A. R. C., Sinha, S., Li, Q., Liu, J., Oh, Y., Müller, D. A., et al. (2024). Simulation-trained machine learning models for quantitative analysis of magnetic skyrmions in Lorentz TEM. *Apl. Mach. Learn.* 2 (2), 026120. doi:10.1063/5.0197138

Mészáros, I. (2007). Development of a novel vibrating sample magnetometer. *Mater. Sci. Forum* 537-538, 413–418. doi:10.4028/www.scientific.net/MSF.537-538.413

Mewes, T., and Mewes, C. K. A. (2021). "Ferromagnetic resonance," in *Magnetic Measurement Techniques for Materials Characterization*. Editors V. Franco, and B. Dodrill (Cham: Springer), 431–452. doi:10.1007/978-3-030-70443-8_16

Mishra, K. K., Lone, A. H., Srinivasan, S., Fariborzi, H., and Setti, G. (2025). Magnetic skyrmion: from fundamental physics to pioneering applications. *Appl. Phys. Rev.* 12 (1), 011315. doi:10.1063/5.0223004

Montoya, E., McKinnon, T., Zamani, A., Girt, E., and Heinrich, B. (2014). Broadband ferromagnetic resonance system and methods for ultrathin magnetic films. *J. Magnetism Magnetic Mater.* 356, 12–20. doi:10.1016/j.jmmm.2013.12.032

Mozooni, B., von Hofe, T., and McCord, J. (2014). Picosecond wide-field magneto-optical imaging of magnetization dynamics of amorphous film elements. *Phys. Rev. B* 90 (5), 054410. doi:10.1103/PhysRevB.90.054410

Mydosh, J. A. (1993). *Spin glasses: An Experimental Introduction*. London: CRC Press.

Nazaretski, E., Martin, I., Movshovich, R., Pelekhov, D., Hammel, P., Zalalutdinov, M., et al. (2007a). Ferromagnetic resonance force microscopy on a thin permalloy film. *Appl. Phys. Lett.* 90 (23), doi:10.1063/1.2747171

Nazaretski, E., Thompson, J. D., Pelekhov, D., Mewes, T., Wigen, P., Kim, J., et al. (2007b). Magnetic resonance force microscopy studies in a thin permalloy film. *J. Magnetism Magnetic Mater.* 310 (2), e941–e943. doi:10.1016/j.jmmm.2006.10.994

Neudecker, I., Woltersdorf, G., Heinrich, B., Okuno, T., Gubbiotti, G., Back, C., et al. (2006). Comparison of frequency, field, and time domain ferromagnetic resonance methods. *J. Magnetism Magnetic Mater.* 307 (1), 148–156. doi:10.1016/j.jmmm.2006.03.060

Neudert, A., McCord, J., Chumakov, D., Schäfer, R., and Schultz, L. (2005). Small-amplitude magnetization dynamics in permalloy elements investigated by time-resolved wide-field Kerr microscopy. *Phys. Rev. B* 71 (13), 134405. doi:10.1103/PhysRevB.71.134405

Niazi, A., Poddar, P., and Rastogi, A. (2000). A precision, low-cost vibrating sample magnetometer. *Curr. Sci.* 79 (1), 99–109. doi:10.1038/35018119

Nizhankovskii, V. I., and Lugansky, L. B. (2007). Vibrating sample magnetometer with a step motor. *Meas. Sci. Technol.* 18 (5), 1533–1537. doi:10.1088/0957-0233/18/5/044

Nosrati, H., Salehiabar, M., Manjili, H. K., Danafar, H., and Davaran, S. (2018). Preparation of magnetic albumin nanoparticles via a simple and one-pot desolvation and co-precipitation method for medical and pharmaceutical applications. *Int. J. Biol. Macromol.* 108, 909–915. doi:10.1016/j.ijbiomac.2017.10.180

Ohldag, H., Van der Laan, G., and Arenholz, E. (2009). Correlation of crystallographic and magnetic domains at Co/NiO(001) interfaces. *Phys. Rev. B* 79, 052403. doi:10.1103/PhysRevB.79.052403

O'Grady, K., Lewis, V. G., and Dickson, D. P. E. (1993). Alternating gradient force magnetometry: applications and extension to low temperatures (invited). *J. Appl. Phys.* 73 (10), 5608–5613. doi:10.1063/1.353613

Palotás, K., Rózsa, L., Simon, E., Udvardi, L., and Szunyogh, L. (2017). Spin-polarized scanning tunneling microscopy characteristics of skyrmionic spin structures exhibiting various topologies. *Phys. Rev. B* 96 (2), 024410. doi:10.1103/PhysRevB.96.024410

Pan, F., Song, C., Liu, X. J., Yang, Y. C., and Zeng, F. (2008). Ferromagnetism and possible application in spintronics of transition-metal-doped ZnO films. *Mater. Sci. Eng. R Rep.* 62 (1), 1–35. doi:10.1016/j.mser.2008.04.002

Patton, C. E., and Kohane, T. (1972). Ultrasensitive technique for microwave susceptibility determination Down to 10^{-5}. *Rev. Sci. Instrum.* 43 (1), 76–79. doi:10.1063/1.1685449

Pelliccione, M., Jenkins, A., Ovartchaiyapong, P., Reetz, C., Emmanouilidou, E., Ni, N., et al. (2016). Scanned probe imaging of nanoscale magnetism at cryogenic temperatures with a single spin quantum sensor. *Nat. Nanotechnol.* 11, 700–705. doi:10.1038/nnano.2016.68

Peng, L., Zhang, Y., Zuo, S., He, M., Cai, J., Wang, S., et al. (2018). Lorentz transmission electron microscopy studies on topological magnetic domains. *Chin. Phys. B* 27 (6), 066802. doi:10.1088/1674-1056/27/6/066802

Peng, Y., Malinowski, G., Gorchon, J., Hohlfeld, J., Salomoni, D., Buda-Prejbeanu, L. D., et al. (2023a). Single-Shot Helicity-Independent all-optical switching in Co/Ho multilayers. *Phys. Rev. Appl.* 20 (1), 014068. doi:10.1103/PhysRevApplied.20.014068

Peng, Y., Malinowski, G., Zhang, W., Lacour, D., Montaigne, F., Mangin, S., et al. (2023b). Laser single-shot magnetization reversal in $Co_{1-x}Lu_x$ nanostructures. *Phys. Rev. B* 107 (21), 214415. doi:10.1103/PhysRevB.107.214415

Peng, Y., Salomoni, D., Malinowski, G., Zhang, W., Hohlfeld, J., Buda-Prejbeanu, L. D., et al. (2023c). In-plane reorientation induced single laser pulse magnetization reversal. *Nat. Commun.* 14 (1), 5000. doi:10.1038/s41467-023-40721-z

Peng, Y., Malinowski, G., Kunyangyuen, B., Salomoni, D., Igarashi, J., Lin, J. X., et al. (2024). From toggle to precessional single laser pulse switching. *Appl. Phys. Lett.* 124 (2), 022405. doi:10.1063/5.0180359

Pham, V. T., Sisodia, N., Di Manici, I., Urrestarazu-Larrañaga, J., Bairagi, K., Pelloux-Prayer, J., et al. (2024). Fast current-induced skyrmion motion in synthetic antiferromagnets. *Science* 384 (6693), 307–312. doi:10.1126/science.add5751

Porthun, S., Rührig, M., and Lodder, J. C. (1995). "Magnetic force microscopy on thin film magnetic recording media," in *Forces in scanning probe methods*. Editors H. J. Güntherodt, D. Anselmetti, and E. Meyer (Dordrecht: Springer Netherlands), 471–476.

Price, N. W., Johnson, R. D., Saenrang, W., Maccherozzi, F., Dhesi, S. S., Bombardi, A., et al. (2016). Coherent magnetoelastic domains in multiferroic $BiFeO_3$films. *Phys. Rev. Lett.* 117 (17), 177601. doi:10.1103/physrevlett.117.177601

Qiu, Z. Q., and Bader, S. D. (2000). Surface magneto-optic Kerr effect. *Rev. Sci. Instrum.* 71 (3), 1243–1255. doi:10.1063/1.1150496

Ramakrishna, A., Murali, N., Mammo, T. W., Samatha, K., and Veeraiah, V. (2018). Structural and DC electrical resistivity, magnetic properties of $Co_{0.5}M_{0.5}Fe_2O_4$ (M= Ni, Zn, and Mg) ferrite nanoparticles. *Phys. B Condens. Matter* 534, 134–140. doi:10.1016/j.physb.2018.01.033

Richter, H. J., Hempel, K. A., and Pfeiffer, J. (1988). Improvement of sensitivity of the vibrating reed magnetometer. *Rev. Sci. Instrum.* 59 (8), 1388–1393. doi:10.1063/1.1139674

Riordan, E., Gozzelino, L., Laviano, F., Napolitano, A., Ghigo, G., Fracasso, M., et al. (2019). Design and implementation of a low temperature, inductance based high frequency alternating current susceptometer. *Rev. Sci. Instrum.* 90 (7), 073908. doi:10.1063/1.5074154

Rodríguez, L. A., Bran, C., Reyes, D., Berganza, E., Vázquez, M., Gatel, C., et al. (2016). Quantitative nanoscale magnetic study of isolated diameter-modulated FeCoCu nanowires. *Am. Chem. Soc. Nano* 10 (10), 9669–9678. doi:10.1021/acsnano.6b05496

Rondin, L., Tetienne, J. P., Hingant, T., Roch, J. F., Maletinsky, P., and Jacques, V. (2014). Magnetometry with nitrogen-vacancy defects in diamond. *Rep. Prog. Phys.* 77 (5), 056503. doi:10.1088/0034-4885/77/5/056503

Roos, W., Hempel, K. A., Voigt, C., Dederichs, H., and Schippan, R. (1980). High sensitivity vibrating reed magnetometer. *Rev. Sci. Instrum.* 51 (5), 612–613. doi:10.1063/1.1136264

Rugar, D., Mamin, H., Erlandsson, R., Stern, J., and Terris, B. (1988). Force microscope using a fiber-optic displacement sensor. *Rev. Sci. Instrum.* 59 (11), 2337–2340. doi:10.1063/1.1139958

Ryu, K. S., Thomas, L., Yang, S. H., and Parkin, S. (2013). Chiral spin torque at magnetic domain walls. *Nat. Nanotechnol.* 8 (7), 527–533. doi:10.1038/nnano.2013.102

Sakar, B., Liu, Y., Sievers, S., Neu, V., Lang, J., Osterkamp, C., et al. (2021). Quantum calibrated magnetic force microscopy. *Phys. Rev. B* 104 (21), 214427. doi:10.1103/PhysRevB.104.214427

Sankey, J., Braganca, P., Garcia, A., Krivorotov, I., Buhrman, R., and Ralph, D. (2006). Spin-transfer-driven ferromagnetic resonance of individual nanomagnets. *Phys. Rev. Lett.* 96 (22), 227601. doi:10.1103/PhysRevLett.96.227601

Sawicki, M., Stefanowicz, W., and Ney, A. (2011). Sensitive SQUID magnetometry for studying nanomagnetism. *Semicond. Sci. Technol.* 26 (6), 064006. doi:10.1088/0268-1242/26/6/064006

Schäfer, R., and McCord, J. (2021). "Magneto-optical microscopy," in *Magnetic measurement techniques for materials characterization*. Editors V. Franco, and B. Dodrill (Cham: Springer International Publishing), 171–229.

Schäfer, S., Pachauri, N., Mewes, C., Mewes, T., Kaiser, C., Leng, Q., et al. (2012). Frequency-selective control of ferromagnetic resonance linewidth in magnetic multilayers. *Appl. Phys. Lett.* 100 (3), 032402. doi:10.1063/1.3678025

Schirhagl, R., Chang, K., Loretz, M., and Degen, C. L. (2014). Nitrogen vacancy centers in diamond: nanoscale sensors for physics and biology. *Annu. Rev. Phys. Chem.* 65, 83–105. doi:10.1146/annurev-physchem-040513-103659

Schmelz, M., Zakosarenko, V., Chwala, A., Schönau, T., Stolz, R., Anders, S., et al. (2016). Thin-film-based ultralow noise SQUID magnetometer. *IEEE Trans. Appl. Supercond.* 26 (5), 1–5. doi:10.1109/TASC.2016.2530699

Schoenenberger, C., Alvarado, S. F., Lambert, S. E., and Sanders, I. L. (1991). Magnetic force microscopy and its application to longitudinal thin films. *J. Magnetism Magnetic Mater.* 93, 123–127. doi:10.1016/0304-8853(91)90315-2

Schönenberger, C., and Alvarado, S. (1989). A differential interferometer for force microscopy. *Rev. Sci. Instrum.* 60 (10), 3131–3134. doi:10.1063/1.1140543

Schütz, G., Wagner, W., Wilhelm, W., Kienle, P., Zeller, R., Frahm, R., et al. (1987). Absorption of circularly polarized x rays in iron. *Phys. Rev. Lett.* 58 (7), 737–740. doi:10.1103/PhysRevLett.58.737

Schwarz, A., and Wiesendanger, R. (2008). Magnetic sensitive force microscopy. *Nano Today* 3 (1-2), 28–39. doi:10.1016/S1748-0132(08)70013-6

Sharma, V., and Kuanr, B. K. (2018). Magnetic and crystallographic properties of rare-earth substituted yttrium-iron garnet. *J. Alloys Compd.* 748, 591–600. doi:10.1016/j.jallcom.2018.03.086

Smith, M., Bull, C., Spink, M. C., Nutter, P., Allen, C. S., Hopkinson, D., et al. (2023). "Optimisation of perpendicular magnetic tunnel junction structures using scanning transmission electron microscopy," in *2023 IEEE international magnetic conference-short papers (INTERMAG short papers)*. New Jersey: IEEE. 1–2.

Soldatov, I. V., and Schäfer, R. (2017). Advanced MOKE magnetometry in wide-field Kerr-microscopy. *J. Appl. Phys.* 122 (15), 153906. doi:10.1063/1.5003719

Spethmann, J., Khanh, N. D., Yoshimochi, H., Takagi, R., Hayami, S., Motome, Y., et al. (2024). SP-STM study of the multi-Q phases in $GdRu_2Si_2$. *Phys. Rev. Mater.* 8 (6), 064404. doi:10.1103/PhysRevMaterials.8.064404

Srivastava, A., Cole, K., Wadsworth, A., Burton, T., Mewes, C., Mewes, T., et al. (2020). Broadband characterization of stress induced anisotropy in nanocomposite $Co_{74.6}Fe_{2.7}Mn_{2.7}Nb_4Si_2B_{14}$. *J. Magnetism Magnetic Mater.* 500, 166307. doi:10.1016/j.jmmm.2019.166307

Stamenov, P., and Coey, J. M. D. (2006). Sample size, position, and structure effects on magnetization measurements using second-order gradiometer pickup coils. *Rev. Sci. Instrum.* 77 (1), 015106. doi:10.1063/1.2149190

Şuan, M. M., Chin, C. K., Abd Razak, J., Hasib, H., Abid, M. A. M., and Nurdin, I. (2020). Synthesis and characterizations of Fe_3O_4 added with Al_2O_3 nanoparticles via sol-gel technique. *IOP Conf. Ser. Mater. Sci. Eng.* 957, 012040. doi:10.1088/1757-899X/957/1/012040

Sun, Y., Lin, T., Lei, N., Chen, X., Kang, W., Zhao, Z., et al. (2023). Experimental demonstration of a skyrmion-enhanced strain-mediated physical reservoir computing system. *Nat. Commun.* 14 (1), 3434. doi:10.1038/s41467-023-39207-9

Sushkov, A. O., Lovchinsky, I., Chisholm, N., Walsworth, R. L., Park, H., and Lukin, M. D. (2014). Magnetic resonance detection of individual proton spins using quantum reporters. *Phys. Rev. Lett.* 113, 197601. doi:10.1103/PhysRevLett.113.197601

Talapatra, A., Gajera, U., Prasad P, S., Arout Chelvane, J., and Mohanty, J. R. (2023). Understanding the magnetic microstructure through experiments and machine learning algorithms. *ACS Appl. Mater. Interfaces* 15 (1), 50318–50330. doi:10.1021/acsami.2c12848

Tamaru, S., Tsunegi, S., Kubota, H., and Yuasa, S. (2018). Vector network analyzer ferromagnetic resonance spectrometer with field differential detection. *Rev. Sci. Instrum.* 89 (5), 053901. doi:10.1063/1.5022762

Tang, C., Alahmed, L., Mahdi, M., Xiong, Y., Inman, J., McLaughlin, N. J., et al. (2023). Spin dynamics in van der Waals magnetic systems. *Phys. Rep.* 1032, 1–36. doi:10.1016/j.physrep.2023.09.002

Thien, T. D., Van Thang, N., Cham, L. T., Thang, P. D., Co, N. D., Van Duong, P., et al. (2024). Characteristics of $Ni_xCo_xMg_xCu_xZn_{1-4x}O$ nanomaterials: their structural and magnetic properties and functional attributes. *Ceram. Int.* 50 (23), 51087–51097. doi:10.1016/j.ceramint.2024.10.019

Thomas, L., Rahmani, A., Renaudin, P., and Wack, A. (2003). High-sensitivity in-plane vector magnetometry using the alternating gradient force method. *J. Appl. Phys.* 93 (10), 7062–7064. doi:10.1063/1.1555392

Todorovic, M., and Schultz, S. (1998). Miniature high-sensitivity quartz tuning fork alternating gradient magnetometry. *Appl. Phys. Lett.* 73 (24), 3595–3597. doi:10.1063/1.122835

Topping, C., and Blundell, S. (2018). AC susceptibility as a probe of low-frequency magnetic dynamics. *J. Phys. Condens. Matter* 31 (1), 013001. doi:10.1088/1361-648X/aaed96

Tsoi, M., Jansen, A., Bass, J., Chiang, W. C., Tsoi, V., and Wyder, P. (2000). Generation and detection of phase-coherent current-driven magnons in magnetic multilayers. *Nature* 406 (6791), 46–48. doi:10.1038/35017512

Tulapurkar, A., Suzuki, Y., Fukushima, A., Kubota, H., Maehara, H., Tsunekawa, K., et al. (2005). Spin-torque diode effect in magnetic tunnel junctions. *Nature* 438 (7066), 339–342. doi:10.1038/nature04207

Van der Laan, G., and Figueroa, A. I. (2014). X-ray magnetic circular dichroism—a versatile tool to study magnetism. *Coord. Chem. Rev.* 277-278, 95–129. doi:10.1016/j.ccr.2014.03.018

Van der Laan, G., and Hesjedal, T. (2023). X-ray detected ferromagnetic resonance techniques for the study of magnetization dynamics. *Nucl. Instrum. Methods Phys. Res. Sect. B Beam Interact. Mater. Atoms* 540, 85–93. doi:10.1016/j.nimb.2023.04.005

Van der Laan, G., and Thole, B. T. (1991). Strong magnetic x-ray dichroism in 2p absorption spectra of 3d transition-metal ions. *Phys. Rev. B* 43 (16), 13401–13411. doi:10.1103/PhysRevB.43.13401

Van Schendel, P. J. A., Hug, H. J., Hoffmann, R., Martin, S., Kappenberger, P., Lantz, M. A., et al. (2001). "Applications of tip calibration in magnetic force microscopy (MFM)," in *Magnetic storage systems beyond 2000*. Editor G. C. Hadjipanayis (Dordrecht, Netherlands: Springer), 313–316.

Vasile, M., Grigg, D., Griffith, J., Fitzgerald, E., and Russell, P. E. (1991). Scanning probe tip geometry optimized for metrology by focused ion beam ion milling. *J. Vac. Sci. Technol. B Microelectron.* 9 (6), 3569–3572. doi:10.1116/1.585846

Vavassori, P. (2000). Polarization modulation technique for magneto-optical quantitative vector magnetometry. *Appl. Phys. Lett.* 77 (11), 1605–1607. doi:10.1063/1.1310169

Vock, S., Sasvari, Z., Bran, C., Rhein, F., Wolff, U., Kiselev, N. S., et al. (2011). Quantitative magnetic force microscopy study of the diameter evolution of bubble domains in a $(Co/Pd)_{80}$ multilayer. *IEEE Trans. Magnetics* 47 (10), 2352–2355. doi:10.1109/TMAG.2011.2155630

Vonsovskii, S. V. (2013). *Ferromagnetic resonance: the phenomenon of resonant absorption of a high-frequency magnetic field in ferromagnetic substances*. Amsterdam: Elsevier.

Wadley, P., Howells, B., Železný, J., Andrews, C., Hills, V., Campion, R. P., et al. (2016). Electrical switching of an antiferromagnet. *Science* 351 (6273), 587–590. doi:10.1126/science.aab1031

Wang, Y., Xiao, Z., Snezhko, A., Xu, J., Ocola, L. E., Divan, R., et al. (2016). Rewritable artificial magnetic charge ice. *Science* 352, 962–966. doi:10.1126/science.aad8037

Wang, Y., Ramaswamy, R., and Yang, H. (2018). FMR-related phenomena in spintronic devices. *J. Phys. D Appl. Phys.* 51 (27), 273002. doi:10.1088/1361-6463/aac7b5

Wang, Z., Guo, M., Zhou, H., Zhao, L., Xu, T., Tomasello, R., et al. (2020). Thermal generation, manipulation and thermoelectric detection of skyrmions. *Nat. Electron.* 3 (11), 672–679. doi:10.1038/s41928-020-00489-2

Wang, L., Cheng, H., Li, P., Van Hees, Y. L. W., Liu, Y., Cao, K., et al. (2022). Picosecond optospintronic tunnel junctions. *Proc. Natl. Acad. Sci. U. S. A.* 119 (24), e2204732119. doi:10.1073/pnas.2204732119

Weinstock, H. (2002). A review of SQUID magnetometry applied to nondestructive evaluation. *IEEE Trans. Magnetics* 27 (2), 3231–3236. doi:10.1109/20.133898

Wohlhüter, P., Bryan, M., Warnicke, P., Gliga, S., Stevenson, S. E., Heldt, G., et al. (2015). Nanoscale switch for vortex polarization mediated by Bloch core formation in magnetic hybrid systems. *Nat. Commun.* 6, 7836. doi:10.1038/ncomms8836

Wu, Y., Shen, Y., Liu, Z., Li, K., and Qiu, J. (2003). Point-dipole response from a magnetic force microscopy tip with a synthetic antiferromagnetic coating. *Appl. Phys. Lett.* 82 (11), 1748–1750. doi:10.1063/1.1560863

Wu, S., Abe, K., Nakano, T., Mewes, T., Mewes, C., Mankey, G., et al. (2019). Thickness dependence of dynamic magnetic properties of soft (FeCo)-Si alloy thin films. *Phys. Rev. B* 99 (14), 144416. doi:10.1103/PhysRevB.99.144416

Wu, J., Chen, X., Yang, Y., Zhi, Q., Wang, X., Zhang, J., et al. (2021). Application of TEM based on HTS SQUID magnetometer in deep geological structure exploration in the Baiyun Gold Deposit, NE China. *J. Earth Sci.* 32 (1), 1–7. doi:10.1007/s12583-020-1086-3

Xu, Y., Yu, Y., Hui, Y., Su, Y., Cheng, J., Chang, H., et al. (2019). Mapping dynamical magnetic responses of ultrathin micron-size superconducting films using nitrogen-vacancy centers in diamond. *Nano Lett.* 19 (8), 5697–5702. doi:10.1021/acs.nanolett.9b02298

Xue, Q. (2025). Recent developments in Lorentz microscopy. *World Sci. Res. J.* 11 (7), 43–49. doi:10.6911/WSRJ.202507_11(7).0005

Youssif, M., Bahgat, A., and Ali, I. A. (2000). AC magnetic susceptibility technique for the characterization of high temperature superconductors. *Egypt. J. Solids* 23 (2), 231–250. doi:10.21608/ejs.2000.151732

Zakrzewski, J. J., Liberka, M., Wang, J., Chorazy, S., and Ohkoshi, S. I. (2024). Optical phenomena in molecule-based magnetic materials. *Chem. Rev.* 124 (9), 5930–6050. doi:10.1021/acs.chemrev.3c00840

Zhan, X., Duan, H., Wang, W., Yan, C., Chen, L., Wang, H., et al. (2024). Quantifying spin-torque efficiency and magnetoresistance coefficient by microwave photoresistance in spin-torque ferromagnetic resonance. *J. Appl. Phys.* 136 (12), 123903. doi:10.1063/5.0231025

Zhang, Z., Gu, K., Toda, M., and Liao, M. (2025). A perspective on diamond MEMS magnetic sensors. *Appl. Phys. Lett.* 126 (10), 100501. doi:10.1063/5.0255014

Zhou, X. G., Li, H., Matsuda, Y. H., Matsuo, A., Li, W., Kurita, N., et al. (2023). Possible intermediate quantum spin liquid phase in α-$RuCl_3$ under high magnetic fields up to 100 T. *Nat. Commun.* 14 (1), 5613. doi:10.1038/s41467-023-41232-7

Zijlstra, H. (1970). A vibrating reed magnetometer for microscopic particles. *Rev. Sci. Instrum.* 41 (8), 1241–1243. doi:10.1063/1.1684777

Zingsem, N., Ahrend, F., Vock, S., Gottlob, D., Krug, I., Doganay, H., et al. (2017). Magnetic charge distribution and stray field landscape of asymmetric néel walls in a magnetically patterned exchange bias layer system. *J. Phys. D Appl. Phys.* 50 (49), 495006. doi:10.1088/1361-6463/aa94e1